ON LOW-PASS RECONSTRUCTION AND STOCHASTIC MODELING OF PWM
SIGNALS

BY

NOYAN CEM SEVÜKTEKİN

THESIS

Submitted in partial fulfillment of the requirements
for the degree of Master of Science in Electrical and Computer Engineering
in the Graduate College of the
University of Illinois at Urbana-Champaign, 2015

Urbana, Illinois

Adviser:

Professor Andrew C. Singer

Abstract

Mathematical modeling of pulse width modulation (PWM) is given. For a band-limited, finite energy input signal, a PWM generation mechanism is investigated in linear and non-linear blocks separately. Following the common practice, a comparator block with a periodic reference signal is offered as a PWM generator and different sampling methodologies are discussed. For natural sampling, where the input signal is compared to the reference signal directly, lossless sampling conditions are derived. For a sawtooth reference signal, the convergence characteristics between lossless natural sampling and uniform sampling, where a zero-order hold (ZOH) block precedes the comparator, are analyzed. For a given input model, the convergence characteristics are tested with simulations and signal to absolute deviation energy for the difference between natural and uniform sampling is observed for different oversampling levels.

Motivated by the separation of linear and non-linear blocks in PWM generation, a similar method for the analysis at the reconstruction end is pursued. In this pursuit, continuous-time low-pass filtering, preceded by oversampling, is analyzed as a linear suboptimal reconstruction mechanism from a PWM signal. Observing the mapping between input samples and pulse widths, an infinite energy, input-independent, structural component of a PWM signal is revealed. Manipulating the linear nature of the low-pass filtering, and equivalent model is proposed to analyze the finite energy, input-dependent component of the PWM signal separately. Frequency domain analysis for fixed-edge and double-edge PWM orientations and their corresponding input-dependent components are given. Using the frequency domain representations, performance bounds for low-pass reconstruction of a band-limited, finite energy input signal are derived and fundamental trade-offs between generator complexity and distortion attenuation capacity are revealed.

Stochastic modeling of PWM processes for independent identically distributed (i.i.d.) pulse widths is discussed. For a fixed starting model of a PWM process, the violation of wide sense stationarity (WSS) is observed. By introducing a randomized starting point, independent of the pulse widths and uniformly distributed over a symbol interval, a WSS PWM process is constructed and its stochastic characteristics are analyzed. For i.i.d. uniform pulse widths, second moments are simulated revealing a smoothing effect in the double-edge PWM construction, consistent to the frequency domain analysis.

Dedicated to Mom and Dad,

who have always believed in me more than I could ever believe in myself

Table of Contents

Chapter 1

Introduction

Pulse width modulation (PWM) is a time-domain modulation technique which entails embedding the sampled input value into the pulse width of the modulated signal under a bijection defined by the modulator [1]. Scaling the input signal in the span of the PWM generator results in larger pulse widths in the corresponding symbol interval, making PWM generation a non-linear operation. Commonly, this non-linear operation is carried out by a comparator circuitry [2, 3]. The comparator construction allows the modulator to adapt different pulse orientations as well as different sampling methodologies [4]. A PWM generator may adapt what is called uniform sampling, where in each symbol interval the comparator constructs the modulated pulse by comparing the reference signal to a fixed sample value, which corresponds to impulse sampling in the traditional signal processing literature [4, 5].

Alternatively, the PWM generator might compare the input signal to the reference signal directly, which results in what is called natural sampling where the sample values are determined implicitly and the symmetry of the pulses is not guaranteed [4]. As a sampling scheme, natural sampling aims to relax the strict dependence on sampling instances similar to what is discussed in [6–8] and it allows a functional form of the level-crossing problem as in [9–11] only for a monotonically changing level. Therefore, natural sampling allows reduced complexity in the generator end, yet introduces additional requirements on perfect recovery, making the rate of convergence between natural sampling and uniform sampling an important criterion for frequency domain analysis of PWM signals.

The time-domain nature of pulse width modulation has allowed these signals to be utilized in power conversion [12–16], voltage inversion [17–19], audio amplification [20], in addition to optical data storage and communication [21, 22]. Lately, voltage controlled oscillator (VCO) based $\Sigma\Delta$ converters have utilized pulse-width modulation to achieve higher-frequency results in analog to digital and digital to digital conversion [23–25]. Given every rising and falling edge instances, the Nyquist sampling theorem ensures perfect reconstruction of a band-limited, finite energy input signal from its corresponding uniformly sampled PWM signal [4, 5]. However, the exact rising and falling edge instances are commonly unknown, which motivates a search for a practical reconstruction mechanism. Furthermore, the Nyquist sampling theorem alone does

not ensure perfect reconstruction from naturally sampled PWM signals even when all rising and falling edge instances are known. In various works [20, 24, 26], continuous-time low-pass filtering is used as a sub-optimal, linear reconstruction mechanism from PWM signals mainly under sinusoidal excitations. Low-pass filtering allows efficient reconstruction when the input signal is oversampled by the generator. Therefore, it is possible to derive fundamental bounds for distortion attenuation in the oversampling factor for different PWM signals, generated from a band-limited, finite energy input signal, which reveals trade-offs between generator complexity and distortion attenuation capacity.

In this thesis, we first focus on the mathematical modeling of PWM generation, revealing that even though it is possible to generate a PWM directly with the comparator construction, the linear and non-linear operations in PWM generation are separable in analysis. We have further shown that the structures of those blocks are determined by the reference signal, which also determines the pulse orientation of a PWM signal. For lossless natural sampling, we have derived conditions on the reference signal, which ensure that there exists a perfect reconstruction mechanism for pulse width modulation with natural sampling. After observing that a lossless natural sampling reference signal necessarily defines a lossless uniform PWM generator, we have turned our attention to convergence characteristics between natural sampling and uniform sampling for a band-limited, finite energy input signal model. Convergence of natural and uniform sampling has allowed us to proceed with the frequency domain representation of PWM signals where we have utilized the separation between linear and non-linear blocks of the PWM generator to discover the structural component in every PWM signal. Then, we have isolated the structural component from the information bearing component of a PWM signal, which has provided an equivalent analysis strategy for PWM signals. Using the equivalent model for PWM reconstruction, we have derived the frequency domain representation of PWM signals for a band-limited, finite energy input model, which has allowed us to postulate fundamental bounds on performance of low-pass reconstruction from PWM signals. With our intuition from PWM generation as well as the frequency domain representation of PWM signals, we have focused on the stochastic modeling of PWM processes. For a band-limited, WSS input process with independent identically distributed samples, we postulated a randomized starting point PWM process, which is necessarily WSS. Furthermore, irrespective of the sampling methodology, we have shown that, with lossless sampling conditions, a WSS PWM process preserves the input statistics under linear operations depending on the pulse orientation.

Chapter 2

Problem Formulation

Pulse width modulation is a time domain modulation technique which maps the input samples into the pulse widths in each symbol interval under a one-to-one mapping. In every symbol interval of a PWM signal, there exists a fixed point, which determines the structure of the signal. For fixed-edge PWM constructions, pulses either start from a fixed point, which is called trailing-edge PWM (TEPWM) or they end at a fixed point, which is called leading-edge PWM (LEPWM). Alternatively, the fixed point might be the mid-point of each symbol interval, in which case, pulses spread around the fixed point and the signal is called double-edge PWM (DEPWM). For double-edge constructions, there exists an alternative sampling methodology which eliminates the fixed point, causing asymmetric pulses in every symbol interval [4]. In this thesis, we do not analyze the asymmetric PWM constructions.

A PWM generator determines the pulse orientation, which leads to different frequency domain and stochastic characteristics, which we analyze in the subsequent chapters. However, irrespective of the pulse orientation, the time difference between the rising edge and falling edge instances in each symbol interval is determined by an invertible mapping between the symbol interval length and input amplitude range. Therefore, pulse width in a symbol interval is the reflection of the corresponding input sample under the defining mapping. In this sense, a PWM generator is a sampler as well as a modulator.

In this chapter, we first model a PWM generator as a mapping between input samples and pulse widths. Then, we introduce two different sampling mechanisms that a PWM generator may adapt, namely the uniform sampling and the natural sampling. Following the discussion on sampling mechanisms, we prove the necessary and sufficient conditions to make lossless sampling using a PWM generator. Then, we introduce a finite energy band-limited input model and discuss its fundamental characteristics such as the existence of a finite maximum and its convergence rate in the tail regions. With this input model, we analyze the convergence characteristics between natural and uniform input samples and their corresponding sampling instances.

2.1 Mathematical Model of a PWM Generator

The basic idea behind pulse width modulation is to embed the input samples into the pulse widths in every symbol interval with an invertible mapping. In other words, $\forall n \in \mathbb{Z}$, let t_n denote the sequence of consecutive rising edge and falling edge instances of a PWM signal. With the understanding that $\forall n \in \mathbb{Z}$, t_n is a non-decreasing sequence which satisfies $[t_{2n}, t_{2n+1}] \subset [nT_M, (n+1)T_M]$, where T_M is the symbol period, t_n defines a PWM signal perfectly:

$$p(t) = \sum_{n=-\infty}^{\infty} u\left(t - t_{2n}\right) - u\left(t - t_{2n+1}\right) \tag{2.1}$$

Where $u(t)$ is the step function, t_{2n} is the subsequence of t_n representing rising edge instances and t_{2n+1} is the subsequence representing falling edge instances of a PWM signal. By the definition of a PWM signal, there exists an invertible mapping $f(\cdot)\colon \mathscr{D}(f) \to \mathscr{R}(f) = [0, T_M]$, defining the pulse widths w_n:

$$w_n \triangleq f(x_n) = t_{2n+1} - t_{2n} \tag{2.2}$$

Here, x_n are input samples $\forall n \in \mathbb{Z}$ and $\mathscr{D}(\cdot)$ denote the domain of a function and $\mathscr{R}(\cdot)$ denote the range of a function. In order to map input samples into pulse widths with a one-to-one mapping, one should emphasize that $\mathscr{D}(f) \supset \mathscr{R}(x(t))$, that is, the range of the input signal is a subset of the domain of the mapping $f(\cdot)$. Furthermore, the range of the mapping is also closed and $\mathscr{R}(f) = [0, T_M]$ by construction. Since $f(\cdot)$ is a one-to-one mapping with a closed range, it follows that $\mathscr{D}(f)$ is also closed, which imposes that a continuous input signal $x(t) \in \mathscr{L}^{\infty}(\mathbb{R})$. At this point, let $A = C\left\|x\right\|_{\infty}$ for some $C > 1$. In Section 2.2, we propose an input model, for which we derive bounds on A.

With the PWM definition in (2.1) and the input to pulse width mapping in (2.2), a PWM generator is modeled in three steps:

1. An invertible function $f(\cdot)$ maps the input samples $x_n \in [-A, A]$ to the pulse widths $w_n \in [0, T_M]$.

2. The Pulse orientation defines the sequence of rising and falling edge instances t_n from the sequence of pulse widths w_n.

3. The sequence of rising and falling edge instances t_n generates the PWM signal $p(t)$.

The pulse orientation of a PWM signal determines how t_n is constructed from w_n by fixing a point in every symbol interval. On one hand, for TEPWM, the starting point of each symbol interval is fixed, yielding that $t_{2n} = nT_M$ and $t_{2n+1} = nT_M + w_n$ and for LEPWM, the end-point of each symbol interval is fixed, which

4

leads to $t_{2n} = nT_M - w_n$ and $t_{2n+1} = nT_M$. We call TEPWM and LEPWM signals circularly symmetric signals since in each symbol interval, the pulses of TEPWM and LEPWM are symmetric of each other around the axis $t = (n + 0.5)T_M$. On the other hand, for DEPWM, each pulse spreads equally around $t = (n+0.5)T_M$, yielding that $t_{2n} = nT_M - \frac{w_n}{2}$ and $t_{2n+1} = nT_M + \frac{w_n}{2}$. Due to circular symmetry, TEPWM and LEPWM signals, which we call fixed edge PWM constructions, demonstrate similar characteristics in Chapter 3 and Chapter 4, which are different from those of DEPWM. These PWM signals have the following explicit forms:

$$p_{TE}(t) = \sum_{n=-\infty}^{\infty} u\left(t - lT_M\right) - u\left(t - lT_M - w_n\right) \tag{2.3}$$

$$p_{LE}(t) = \sum_{n=-\infty}^{\infty} u\left(t - lT_M + w_n\right) - u\left(t - lT_M\right) \tag{2.4}$$

$$p_{DE}(t) = \sum_{n=-\infty}^{\infty} u\left(t - lT_M + \frac{w_n}{2}\right) - u\left(t - lT_M - \frac{w_n}{2}\right) \tag{2.5}$$

The mapping between t_n and $p(t)$ is commonly realized by a comparator construction with a triangular reference wave [3, 4, 17, 22, 26]. The comparator construction determines the sampling methodology of the input signal and the reference signal of the comparator determines the pulse orientation of the PWM signal. If the input signal $x(t)$ is compared to a periodic reference signal $r(t)$ directly, it is called natural sampling where the relation between input samples x_n and pulse widths w_n is given implicitly. If the comparator is preceded by a zero-order hold (ZOH) block, then it is called uniform sampling and in that case, the input samples are mapped to pulse widths explicitly. Figures 2.1–2.3 illustrate the generation of uniformly sampled PWM signals with a triangular reference signal, where output of the ZOH block, denoted by $x_{ZOH}(t)$, has the following structure:

$$x_{ZOH}(t) = \sum_{n=-\infty}^{\infty} x(nT_M)\left[u(t - nT_M) - u(t - (n+1)T_M)\right] \tag{2.6}$$

In the uniform sampling case, for a given construction, the PWM generator constructs the width of the PWM signal by comparing $x(nT_M)$ with $r(t)$ in every symbol interval $[nT_M, (n+1)T_M]$. If a triangular reference signal is used to generate a uniformly sampled PWM signal, then, $f(\cdot)$ is an affine mapping and the equation between w_n and $x_n = x(nT_M)$ is explicit and affine. We allow the following affine mapping to define the PWM generator and its corresponding reference signals:

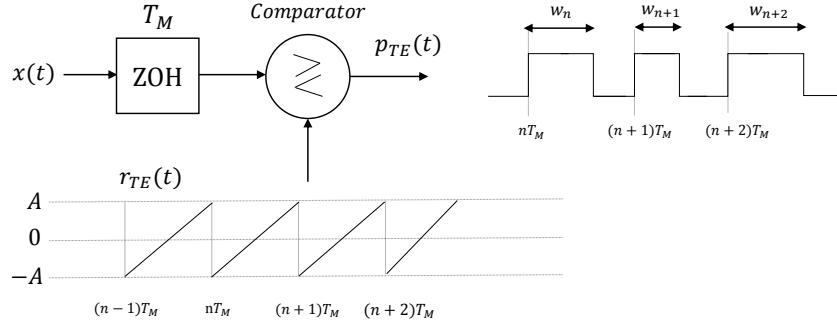$$w_n = \frac{T_M}{2A}\left(x_n + A\right) \tag{2.7}$$

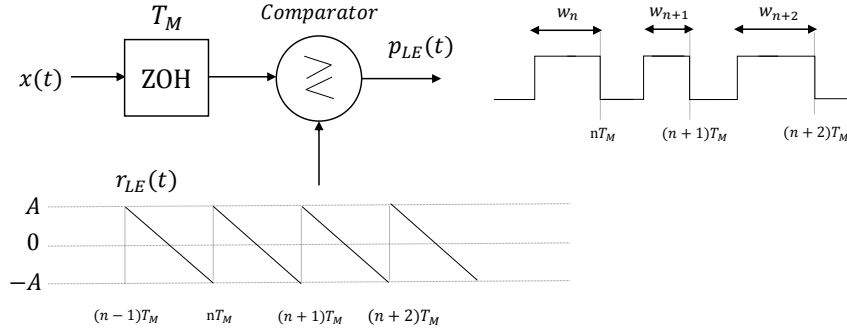Figure 2.1: Uniformly Sampled TEPWM Construction

Figure 2.2: Uniformly Sampled LEPWM Construction

The mapping $f(x) = \frac{T_M}{2A}(x + A)$ is an affine mapping, which is invertible and continuous. We allow the domain of the mapping $\mathscr{D}(f) = [-A, A]$, then, $\mathscr{R}(f) = [0, T_M]$ since $f(\cdot)$ is continuous. Allowing $t_{T_M} = t \mod T_M$, the sawtooth reference signals for different PWM constructions, which provide the mapping in (2.7), are as follows:

$$r_{TE}(t) = \frac{2A}{T_M}t_{T_M} - A \tag{2.8}$$

$$r_{LE}(t) = A - \frac{2A}{T_M}t_{T_M} \tag{2.9}$$

$$r_{DE}(t) = \begin{cases} \frac{4A}{T_M}t_{T_M} - A & \text{if } t_{T_M} < \dfrac{T_M}{2} \\ 3A - \frac{4A}{T_M}t_{T_M} & \text{if } t_{T_M} \geq \dfrac{T_M}{2} \end{cases} \tag{2.10}$$

As an alternative to uniform sampling, the generator complexity can be reduced in the expense of implicitly determined input samples by adapting natural sampling instead. Figures 2.4–2.6 illustrate PWM generation using natural sampling. In the natural sampling, the intersection point between the input signal
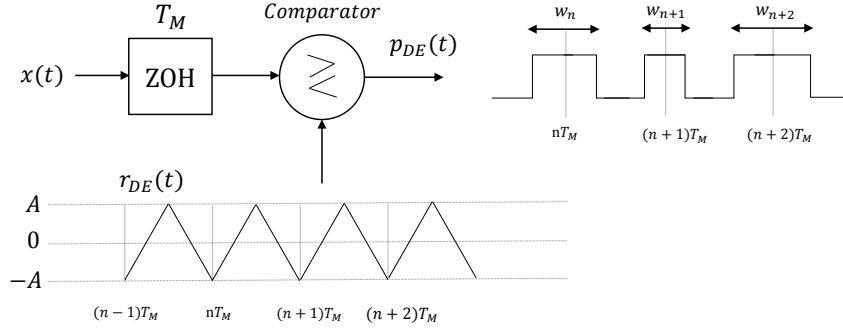
Figure 2.3: Uniformly Sampled DEPWM Construction

and the reference signal in each symbol interval determines the corresponding pulse width as a result of the following implicit equation:

$$r(w_n) = x(nT_M + w_n) \tag{2.11}$$

In the uniform sampling, the ZOH block ensures the existence and uniqueness of the intersection point in every symbol interval since $x_{ZOH}(t) = x(nT_M)$, $\forall t \in [nT_M, (n+1)T_M]$. However, in the natural sampling, a unique intersection point does not necessarily exist in every symbol interval. With the understanding that a PWM generator is inherently a sampler, we now establish the framework to propose the lossless sampling conditions for a PWM generator.

Until this point, the nature of PWM generation has only imposed that the input signal $x(t) \in \mathscr{L}^\infty(\mathbb{R})$ is continuous. This is a necessary condition to ensure one-to-one mapping between input samples and pulse widths, or equivalently to avoid clipping in the output. However, in order to evaluate PWM generation as a sampling mechanism, we impose two further conditions:

1. The input signal is band-limited: $x(t) \in \mathcal{BL}[-\Omega_0, \Omega_0]$.

2. The input signal is finite energy: $x(t) \in \mathscr{L}^2(\mathbb{R})$.

The first condition follows from conventional sampling theory as in [5, 27, 28] and provides us with the framework to reconstruct the signal from the samples, $x_n = f^{-1}(w_n)$. In other words, if pulse widths w_n were given to the reconstruction mechanism, the first condition would be enough to reconstruct the original signal. However, the reconstruction mechanism only has $p(t)$ and it is not always possible to recover w_n perfectly from the PWM signal, which leads us to impose the latter condition. In Chapter 3, we analyze the performance of continuous time low-pass filtering as a suboptimal reconstruction mechanism from PWM signals where we show that the distortion energy due to low-pass filtering is bounded for a finite energy input signal.

7
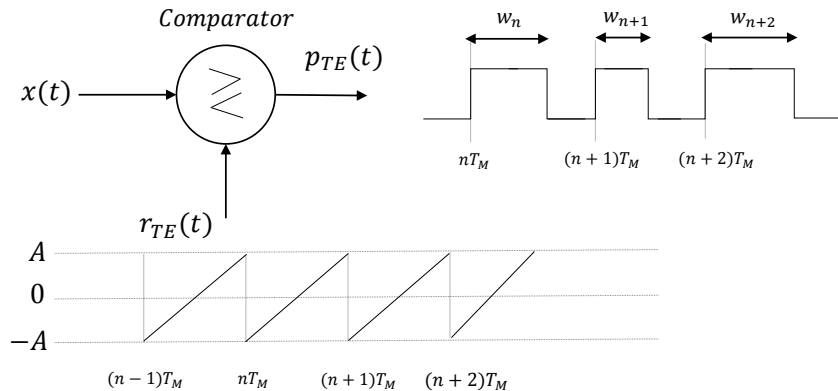
Figure 2.4: Naturally Sampled TEPWM Construction
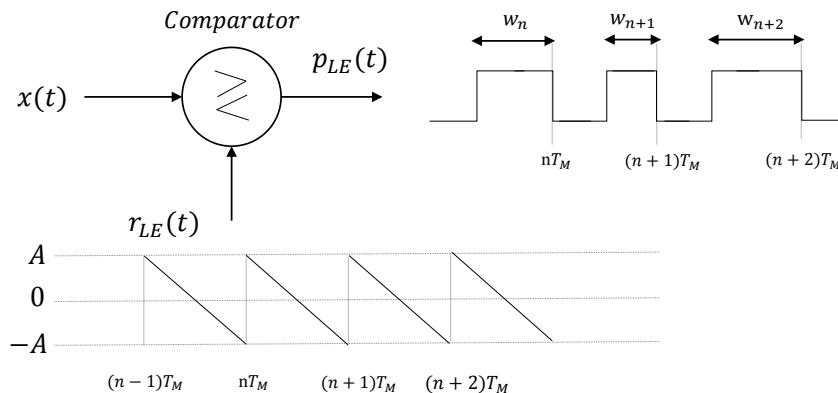
Figure 2.5: Naturally Sampled LEPWM Construction

Once $x(t) \in \mathcal{BL}\left[-\Omega_0, \Omega_0\right]$, we let $\Omega_0 = \frac{\pi}{T}$, which yields that T is the Nyquist sampling period for the band-limited input signal. As we will show in Chapter 3, the distortion energy due to suboptimal reconstruction diminishes in the oversampling factor M. Therefore, for any PWM signal, we define the symbol interval, T_M, as the oversampling period:

$$T_M = \frac{T}{M} \tag{2.12}$$

A PWM generator is not a sampler in the conventional sampling sense, because $\forall n$, the input samples are mapped to separation times between rising edges t_{2n} and falling edges t_{2n+1} rather than the amplitude of the sampled signal. Therefore, the symbol interval of a PWM signal, which is determined by the period of the reference signal, is the sampling period in the mainstream sampling theory. With this understanding, Theorem 2.1.1 establishes the necessary and sufficient conditions for lossless natural sampling using a PWM

Figure 2.6: Naturally Sampled DEPWM Construction

generator:

Theorem 2.1.1. *Let a finite energy band-limited signal $x(t)$ of band-width $[-\Omega_0, \Omega_0]$, with $\Omega_0 = \frac{\pi}{T}$, be compared to a periodic triangular reference signal $r(t) = \frac{2A}{T_r} t_{T_r} - A$, where $t_{T_r} = t \mod T_r$. Then,*
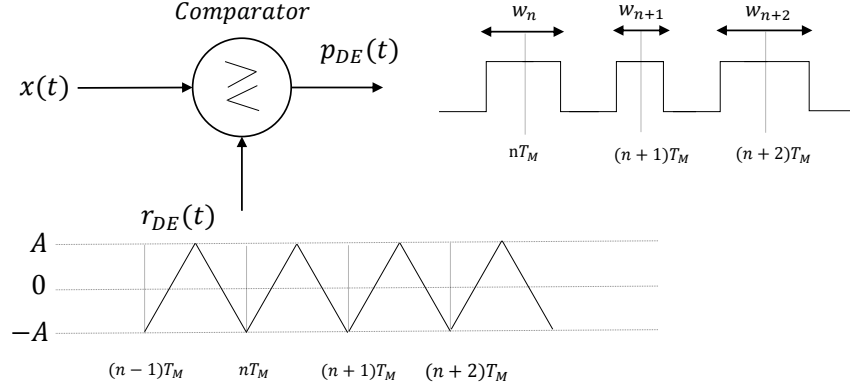
1. *$\|x\|_\infty \leq A$ ensures the existence of an intersection point in $[nT_r, (n+1)T_r]$, $\forall n \in \mathbb{Z}$.*

2. *Allowing $A = C \|x\|_\infty$ for a finite constant $C \geq \frac{\pi}{2}$, period of the reference signal, T_r, satisfying the Nyquist sampling condition for the band-limited signal $x(t)$ ensures uniqueness of the existence point.*

These two conditions together allow the input signal to be lossless (Nyquist) naturally sampled.

Proof. For the first requirement, we first observe that in every symbol interval $[nT_r, (n+1)T_r]$, $r(t) \in [-A, A]$, since $r(t)$ is periodic, the range of the reference signal $\mathscr{R}\{r(t)\} = [-A, A]$. Then $\|x\|_\infty \leq A$ allows $\mathscr{R}\{x(t)\} \subset \mathscr{R}\{r(t)\}$. Since in each symbol interval, $r(t)$ monotonically spans $\mathscr{R}\{r(t)\}$, it spans $\mathscr{R}\{x(t)\}$ as well, which yields the existence of the intersection point.

For the second requirement, we first prove that a band-limited finite energy signal is necessarily bounded. The proof follows from the Cauchy-Schwarz inequality. First, let us observe the inverse Fourier transform:

$$x(t) = \frac{1}{2\pi} \int_{-\infty}^{\infty} X(j\Omega) e^{j\Omega t} \, d\Omega = \frac{1}{2\pi} \int_{-\Omega_0}^{\Omega_0} X(j\Omega) e^{j\Omega t} \, d\Omega$$

Taking the absolute value yields:

$$|x(t)| = \frac{1}{2\pi} \left| \int_{-\Omega_0}^{\Omega_0} X(j\Omega) e^{j\Omega t} \, d\Omega \right| \leq \frac{1}{2\pi} \int_{-\Omega_0}^{\Omega_0} \left| X(j\Omega) e^{j\Omega t} \right| \, d\Omega = \frac{1}{2\pi} \int_{-\Omega_0}^{\Omega_0} |X(j\Omega)| \, d\Omega$$

9

Then, the Cauchy-Schwarz inequality on the last integral yields that $|x(t)|$ is bounded by the following:

$$|x(t)| \leq \frac{\sqrt{2\Omega_0}}{2\pi} \sqrt{\int_{-\Omega_0}^{\Omega_0} |X(j\Omega)|^2 \, d\Omega}$$

Since $x(t)$ is finite energy, $E_X = \frac{1}{2\pi} \int_{-\Omega_0}^{\Omega_0} |X(j\Omega)|^2 \, d\Omega$ and $\Omega_0 = \frac{\pi}{T}$,

$$|x(t)| \leq \sqrt{\frac{E_X}{T}}$$

Therefore, $x(t) \in \mathscr{L}^\infty(\mathbb{R})$. The rest of the proof is by contradiction. Assume that $\exists t_1 \neq t_2 \in [0, T_r]$ such that $x(t_1) = r(t_1)$ and $x(t_2) = r(t_2)$. Without loss of generality allow $t_1 < t_2$, which yields that $r(t_1) < r(t_2)$. Then, by the mean value theorem, $\exists t_3 \in [t_1, t_2]$ such that:

$$\frac{dx}{dt}\bigg|_{t_3} = \frac{x(t_2) - x(t_1)}{t_2 - t_1} = \frac{r(t_2) - r(t_1)}{t_2 - t_1} = \frac{2A}{T_r} \tag{2.13}$$

Now, we show that $\frac{2A}{T_r} > \left\| \frac{dx}{dt} \right\|_\infty$, which will conclude the contradiction. This follows from the inverse Fourier transform of the $\frac{dx}{dt}$:

$$\left| \frac{dx}{dt} \right| = \left| \frac{1}{2\pi} \int_{-\Omega_0}^{\Omega_0} j\Omega X(j\Omega) e^{j\Omega t} \, d\Omega \right| = \left| \frac{1}{2\pi} \int_{-\Omega_0}^{\Omega_0} \Omega X(j\Omega) e^{j\Omega t} \, d\Omega \right|$$

On a compact interval I, two continuous functions $f(\cdot)$ and $g(\cdot)$ satisfy:

$$\int_I f(x)g(x) \, dx \leq \max_{x \in I} |g(x)| \int_I g(x) \, dx$$

Therefore,

$$\left| \frac{dx}{dt} \right| \leq \left| \frac{1}{2\pi} \int_{-\Omega_0}^{\Omega_0} \Omega_0 X(j\Omega) e^{j\Omega t} \, d\Omega \right|$$

Since $\|x\|_\infty$ is bounded,

$$\left| \frac{dx}{dt} \right| \leq \Omega_0 \, |x(t)| \leq \Omega_0 \, \|x\|_\infty$$

Since $\Omega_0 = \frac{\pi}{T}$, the Nyquist sampling period is T. Therefore,

$$\frac{2A}{T_r} = \frac{2C \, \|x\|_\infty}{T_r} \geq \frac{\pi \, \|x\|_\infty}{T_r} = \Omega_0 \, \|x\|_\infty \left(\frac{T}{T_r} \right) \geq \left\| \frac{dx}{dt} \right\|_\infty \left(\frac{T}{T_r} \right)$$

Since T_r satisfies the Nyquist sampling condition, $T_r \leq T$, but then $\left(\frac{T}{T_r} \right) \geq 1$, yielding that $\exists t_3$ such that $\frac{dx}{dt}\big|_{t_3} > \left\| \frac{dx}{dt} \right\|_\infty$, which is a contradiction. Therefore, the intersection point in each symbol interval is unique. Finally, one-to-one mapping between the lossless uniform samples and the intersection points in every symbol
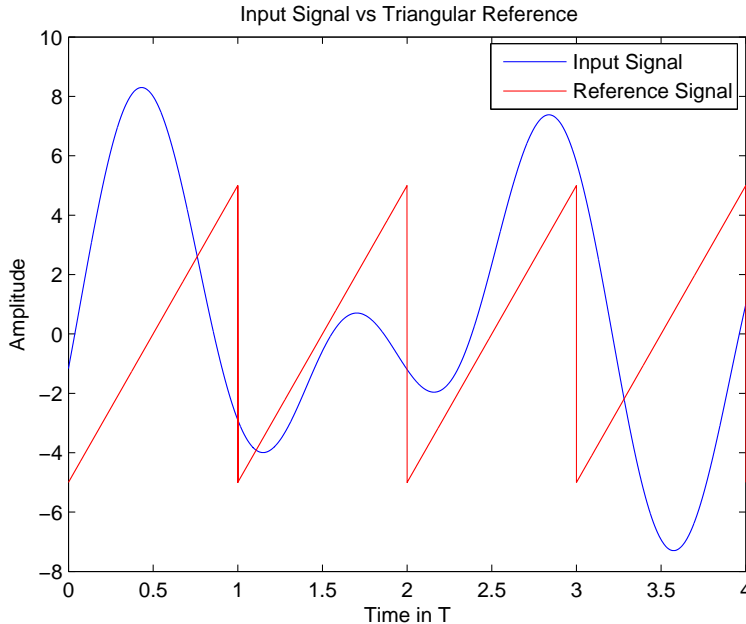
Figure 2.7: No Intersection between Input Signal and Reference Signal in the Symbol Interval $[2T_r, 3T_r]$

interval yields that $r(t)$ ensures lossless natural sampling. □

One should emphasize that even though Theorem 2.1.1 uses (2.8) as the reference signal, the results apply for reference signals in (2.9) and (2.10) as well. The first lossless sampling condition ensures that there is no clipping of the input signal, which is equivalent to the existence of the intersection points between $r(t)$ and $x_{ZOH}(t)$ for uniform sampling and between $r(t)$ and $x(t)$ for natural sampling, as opposed to what is illustrated in Fig. 2.7. The latter condition imposes that there is a one-to-one correspondence between input samples and pulse widths, or equivalently, the uniqueness of the intersection point in each symbol interval as opposed to what is illustrated in Fig. 2.8. With the oversampling factor $M \geq 1$, our mapping in (2.7) and with the understanding that $A = C \|x\|_\infty$ for some $C \geq \frac{\pi}{2}$, lossless sampling conditions are satisfied, which yields that $\forall n \in \mathbb{Z}$, $\exists w_n [0, T_M]$, unique such that (2.11) holds.

We conclude this section with two important remarks on the nature of PWM signals. First, even when the input signal, $x(t) \in \mathscr{L}^2(\mathbb{R})$, the corresponding PWM signal is not finite energy, that is, $p(t) \notin \mathscr{L}^2(\mathbb{R})$, since it carries a DC component that the mapping in (2.7) introduces. In other words, if perfect recovery is done from a PWM signal, the recovered signal $w(t) = f(x(t))$, and $w(t) \notin \mathscr{L}^2(\mathbb{R})$ due to the DC component from $f(\cdot)$. This causes $p(t)$ to not converge uniformly to 0 in pulse energy, which yields that the frequency domain representation of $p(t)$ is not well defined without impulsive components. This fact motivates us to propose a separation approach in Chapter 3, which allows us to separate finite energy input dependent

11
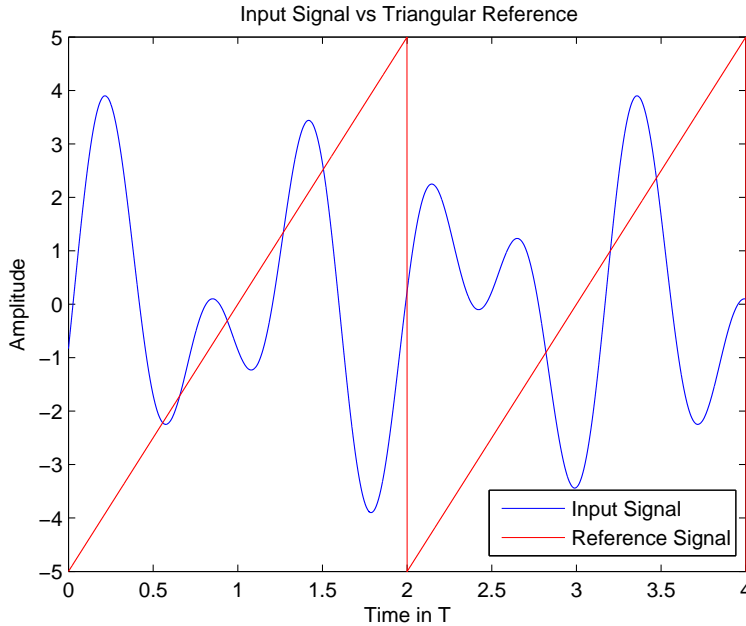
Figure 2.8: Non-unique Intersection between Input Signal and Reference Signal in a Symbol interval

components from infinite energy structural components.

The second remark is closely related to the reason for using a continuous time low-pass filter as a suboptimal reconstruction mechanism. Even though the input signal is band-limited, the PWM signal is necessarily not band-limited, which makes the sampling of the PWM signal an inherently faulty operation. However, the distortion due to the sampling of the PWM signal manifests itself in a unique way; sampling a PWM signal is equivalent to quantization of the input signal. In this thesis, we postulate the performance bounds on suboptimal reconstruction from uniformly sampled PWM signals in the so-called best case, which entails using a continuous time low-pass filter as the reconstruction mechanism, therefore, we will not introduce any quantization effect.

In Section 2.2, we propose an input model, which satisfies the input signal requirements of this section. Then, we derive bounds on its fundamental characteristics, which we use to investigate the convergence characteristics between uniform sampling and natural sampling. We show that as the input signal, $x(t) \to 0$, the uniform samples and natural samples converge to each other as the difference between their sampling instances converges to a finite constant, which defines the infinite energy, input independent, structural signal component that we separate in Chapter 3.

2.2 Convergence of Uniform and Natural Sampling

As the input model for our analysis, we propose an input signal $x(t) \in \mathscr{S}_N$, where $\mathscr{S}_N$ is an N-dimensional, orthogonal, band-limited signal space spanned by the basis functions $\phi_k(t) = \mathrm{sinc}\,(\Omega_0(t - kT))$ for $k \in [0, N-1]$:

$$x(t) = \sum_{k=0}^{N-1} c_k \phi_k(t) \tag{2.14}$$

where, $\Omega_0 = \frac{\pi}{T}$, yielding that $x(t) \in \mathcal{BL}[-\Omega_0, \Omega_0]$. Furthermore, $\mathrm{sinc}(x) = \frac{\sin(x)}{x}$ thus, the basis functions satisfy:

$$\langle \phi_k, \phi_l \rangle = \int_{-\infty}^{\infty} \phi_k(t)\phi_l(t)\, dt = \delta_{k-l} \tag{2.15}$$

where δ_{k-l} is the Kronecker delta function. In order to ensure that $x(t) \in \mathscr{L}_2(\mathbb{R})$, it is necessary to have $\mathbf{c} = [c_0, .., c_{N-1}]^T$ satisfy $\|\mathbf{c}\|_\infty \leq \infty$, which follows from $\mathscr{S}_N$ being a signal space. Yet, we further impose a normalization condition which ensures that $\|\mathbf{c}\|_\infty = 1$, this condition normalizes the amplitude bounds which would otherwise depend on $\|\mathbf{c}\|_\infty$. We should emphasize here that (2.14) represents a wide variety of practical signals; any band-limited and finite energy signal can be projected onto $\mathscr{S}_N$ and represented as in (2.14) within an minimum square error after normalization.

The input signal in (2.14) is an element of an N-dimensional space spanned by $\{\phi_k\}_{k=0}^{N-1}$, and $\forall k \in \mathbb{Z}$, $|\phi_k(t)| \leq \frac{1}{|t|}$, $\forall t \in \mathbb{R}$. Since the input signal model is not symmetrical, we define the right-hand side tail of $x(t)$ to start at $t = NT$ and the left-hand side tail to end at $t = -T$. We upper-bound the input signal in the tail regions as a function of t, which allows us to characterize the convergence between uniform and natural samples. Yet first, we postulate an upper bound on $\max_{t \in \mathbb{R}} |x(t)|$, which is constant in t and is necessary for reference signal construction:

Lemma 2.2.1. *The input signal $x(t)$ as defined in (2.14) is absolutely upper-bounded $\forall N < \infty$:*

$$\max_{t \in \mathbb{R}} \{|x(t)|\} \leq \begin{cases} 1 & \text{if } N = 1 \\ \frac{4}{\pi} \sum_{k=1}^{\frac{N}{2}} \frac{1}{2k-1} & \text{if } N \geq 2 \text{ and } N \text{ is even} \\ \frac{4}{\pi} \left(\sum_{k=1}^{\frac{N+1}{2}} \frac{1}{2k-1} - \frac{1}{2N} \right) & \text{if } N \geq 3 \text{ and } N \text{ is odd} \end{cases} \tag{2.16}$$

Proof. Since $x(t) \in \mathscr{L}^2(\mathbb{R})$, $\exists \|x\|_\infty \leq \infty$. Therefore, we first construct the coefficient sequence $\mathbf{c}$ such that $\max\{|x(t)|\}$ is achievable. It follows from the case where $N = 1$ that the maximum is only achievable on the boundary of $\mathbf{c}$, that is $|c_k| = 1$, $\forall k \in [0, N-1]$. We further observe that for $N = 2$, $\mathbf{x} = [1, 1]^T$ has a maximum of $x(t)$ at $t = \frac{T}{2}$. Since we investigate the $\mathscr{L}_\infty$ norm for the input signal, the polarity of the

13

coefficient vector is not significant. In other words, the positive construction such as $\mathbf{x} = [1, 1]^T$ provides a maximum and we emphasize that without loss of generality, the reversed polarity coefficient vector such as $\mathbf{x} = [-1, -1]^T$, would result in the same absolute maximum. Then, we observe the alternating series structure of the basis functions and construct the coefficient set to superpose the same sign tail components in a single interval. Since $\arg\max_{t \in \mathbb{R}} \{\phi_k(t)\} = kT$, $\forall k \in [0, N-1]$, the following construction achieves the maximum:

1. For $N = 1$, let $c_0 = 1$. Then, $x(0) = 1$ and $\forall c_0 \in [-1, 0)$, $\max \{x(t)\} = x(0) = c_0 < 0$.

2. For $N = 2$, let $\mathbf{c} = [1, 1]^T$. Then, $\arg\max x(t) = \frac{T}{2}$ and $\max \{x(t)\} = \frac{4}{\pi}$.

3. For $N = 2k + 1$ and $k \in \mathbb{N}$, Then,

$$
\mathbf{c} = \begin{cases} [1, ..., 1, 1, ..., 1, -1]^T & \text{if } k \text{ is odd} \\ [-1, ..., 1, 1, ..., -1, 1]^T & \text{if } k \text{ is even} \end{cases}
$$

with, $\arg\max \{x(t)\} = \frac{(N-2)T}{2}$.

4. For $N = 2k + 2$ and $k \in \mathbb{N}$. Then,

$$
\mathbf{c} = \begin{cases} [-1, 1, ..., 1, 1, ..., 1, -1]^T & \text{if } k \text{ is odd} \\ [1, -1, ..., 1, 1, ..., -1, 1]^T & \text{if } k \text{ is even} \end{cases}
$$

with, $\arg\max \{x(t)\} = \frac{(N-1)T}{2}$.

The cases where $N = 1$ and $N = 2$ initiate the symmetric structure of the coefficient vector. Then, we allow that for $N = 3$, $\mathbf{c} = [1, 1, -1]^T$, that is, we initiate the alternating structure from the right hand side.

In the region $t \in [0, T]$, $\mathrm{sinc}(\Omega_0(t - 2T)) > 0$, yielding that $\exists \hat{t} \in [0, T]$: $x(\hat{t}) \geq \frac{4}{\pi}$. Since basis functions are symmetrical, adding $\phi_2(t)$ preserves the maximum achieving point, yielding that $\hat{t} = \arg\max \{x(t)\}$. The same construction applies for any transition except for the fact that the symmetrical construction merely shifts $\arg\max \{x(t)\}$ by T as proposed in the construction. Therefore, the mathematical induction concludes that the proposed construction for the coefficient vector achieves the maximum for the input signal. Then, we show that the given construction, which achieves the absolute maximum for $x(t)$ is upper-bounded by (2.16) for any given N. Since the construction is symmetrical for N even, the absolute maximum has the

14

following form:

$$\max_{t\in\mathbb{R}}\{|x(t)|\} = A = 2\sum_{k=1}^{\frac{N}{2}}\left|\text{sinc}\left(\Omega_0\frac{(2k-1)T}{2}\right)\right| = 2\sum_{k=1}^{\frac{N}{2}}\left|\text{sinc}\left(\frac{(2k-1)\pi}{2}\right)\right|$$

Using the definition of the basis functions yields that and noting that $\left|\sin\left(\frac{n\pi}{2}\right)\right| = 1, \forall n$:

$$= 2\sum_{k=1}^{\frac{N}{2}}\left|\frac{\sin\left(\frac{(2k-1)\pi}{2}\right)}{\Omega_0\frac{(2k-1)T}{2}}\right| \leq 2\sum_{k=1}^{\frac{N}{2}}\left|\frac{1}{\frac{(2k-1)\pi}{2}}\right| = \frac{4}{\pi}\sum_{k=1}^{\frac{N}{2}}\frac{1}{(2k-1)}$$

Then, (2.16) follows from disturbing the symmetry by an additive shifted basis function, which concludes the proof. $\square$

As discussed in Section 2.1, a PWM generator can sample a signal with no loss provided that the input signal range lies within the range of the reference signal within a positive multiplicative factor $C \geq \frac{\pi}{2}$. Lemma 2.2.1 provides a model for the case where the input signal is absolutely upper-bounded, thus, it is possible to analyze lossless sampling. Next, we propose an upper bound for the tail regions, which is required for our analysis on the convergence natural sampling and uniform sampling.

Lemma 2.2.2. *The input signal $x(t)$ as defined in (2.14) is upper-bounded by $|x(t)| \leq \frac{N}{\Omega_0(t-(N-1)T)}$ for $t > NT$ and $|x(t)| \leq \frac{N}{|\Omega_0 t|}$ for $t \leq -T$.*

Proof. The proof begins with the input signal definition:

$$|x(t)| = \left|\sum_{k=0}^{N-1} c_k \text{sinc}\left(\Omega_0\left(t - kT\right)\right)\right|$$

By the triangle inquality over a finite sum, we get:

$$|x(t)| \leq \sum_{k=0}^{N-1} |c_k| \left|\text{sinc}\left(\Omega_0\left(t - kT\right)\right)\right|$$

Since $|\text{sinc}(x)| \leq \frac{1}{x}, \forall x \in \mathbb{R}$ and $\Omega_0 > 0$:

$$|x(t)| \leq \sum_{k=0}^{N-1} \frac{|c_k|}{|\Omega_0\left(t - kT\right)|} = \frac{1}{\Omega_0}\sum_{k=0}^{N-1} \frac{|c_k|}{|t - kT|}$$

$\forall k \in \mathbb{Z}$, we restrict $|c_k| \leq 1$, which yields that:

$$|x(t)| \leq \frac{1}{\Omega_0}\sum_{k=0}^{N-1} \frac{1}{|t - kT|} \tag{2.17}$$

On the right-hand side tail, (2.17) is a finite sum of positive, monotonically increasing elements $\forall t \geq NT$. Therefore, we can use the largest element bound, which is the last element, $k = N - 1$:

$$|x(t)| \leq \frac{N}{\Omega_0\left(t - (N-1)T\right)} = B_r(t) \tag{2.18}$$

15

On the left-hand side tail, (2.17) is a finite sum of positive and monotonically decreasing elements $\forall t \leq -T$. Therefore, we can still use the largest element bound, which is the first element, $k = 0$. In that case:

$$|x(t)| \leq \frac{N}{\Omega_0 |t|} = B_l(t) \tag{2.19}$$

$\square$

With Lemma 2.2.2, the framework for the convergence problem is now established. Next, we use these upper bounds to find the maximum value of a natural sample in each sampling interval and postulate a geometrical approach to find the worst-case absolute separation between natural samples and uniform samples, which is:

$$\Delta_x = |x_U[n] - x_N[n]| \tag{2.20}$$

We further show the convergence between natural sampling instances and uniform sampling instances motivates the separation principle that we discuss in the Chapter 3. It follows from the mapping in (2.7):

$$\Delta_t = \left| t_n - \frac{nT}{M} \right| = \frac{T_M}{2A} |x(t_n) + A| \tag{2.21}$$

The intersection point of an arbitrary band-limited signal and a line equation does not necessarily have a closed-form expression, which is the main difficulty in analyzing the natural sampling. Furthermore, approximating the intersection point requires imposing a restriction on the signal derivative [4]. However, since the lossless sampling criteria ensure that there is only one intersection point in each sampling interval, imposing any further conditions on the input structure is unnecessary. Therefore, we upper-bound the input signal magnitude in the tail regions rather than approximating the input signal at a given instant. Lemma 2.2.3 establishes this geometrical framework.

Lemma 2.2.3. *Let a continuous, finite energy, band-limited signal $s(t)$ be bounded absolutely by some positive, monotonic, convergent upper bound $B(t)$ in its tail regions. Given that the signal is sampled with some T_s that satisfies the lossless sampling conditions, the maximum deviation between the uniform samples $s_U[n] = s(nT_s)$ and natural samples $s_N[n] = s(t_n) = r(t_n)$ is bounded by:*

$$|s_U[n] - s_N[n]| \leq B(\hat{t}_n) + B(nT_s) \tag{2.22}$$

where $\hat{t}_n$ satisfies $B(\hat{t}_n) = r(\hat{t}_n)$. Furthermore, if $s(t)$ has the form in (2.14) and $T_s = \frac{T}{M}$ for some positive

integer M, the bound can be improved as follows:

$$|s_U[n] - s_N[n]| \leq \max\left\{\left|B(\hat{t}_n) - B(nT_s)\right|, \left|B(\hat{t}_n)\right|\right\} \tag{2.23}$$

And the corresponding deviation between sampling instances is bounded by:

$$t_n - nT_s \leq \hat{t}_n - nT_s \tag{2.24}$$

Proof. In a sampling interval $t \in [nT_s, (n+1)T_s]$, the nth natural sample point is the unique intersection point of the sawtooth reference signal, $r(t)$, and the input signal, $s(t)$, where the nth uniform sample is the value of the input signal at the beginning of the sampling interval, at $t = nT_s$. Since $B(t)$ is monotonic, in each symbol interval, $\exists \hat{t}_n$ such that $B(\hat{t}_n) = r(\hat{t}_n)$. Furthermore, $|s(t)| \leq B(t)$ in tail regions, which yields that in tail regions, $-B(nT_s) \leq s(nT_s)$ and $s(t_n) \leq s(\hat{t}_n)$. Therefore,

$$|s_N[n] - s_U[n]| \leq \left| \underbrace{\max_{t \in [nT_s, (n+1)T_s]} s(t)}_{B(\hat{t}_n)} - \underbrace{\min_{t=nT_s} s(t)}_{-B(nT_s)} \right|$$

Furthermore, because of monotonicity of the reference signal, for any possible instant, $\hat{t}_n$, we know that $\hat{t}_n \geq t_n \geq nT_s$. Therefore,

$$t_n - nT_s \leq \hat{t}_n - nT_s$$

However, when the sampling period is chosen as $T_M = \frac{T}{M}$, the input model in (2.14) allows that in each symbol interval $\nexists t_0 : s(t_0) = 0$. In other words, in each symbol interval the sign of the input signal remains the same, which allows that the maximum deviation between uniform and natural samples is bounded either by $\left|B(\hat{t}_n) - B(nT_s)\right|$ or by $\left|B(\hat{t}_n) - 0\right|$, which yields that:

$$|s_U[n] - s_N[n]| \leq \max\left\{\left|B(\hat{t}_n) - B(nT_s)\right|, \left|B(\hat{t}_n)\right|\right\} \tag{2.25}$$

$\square$

Lemma 2.2.3 provides $B(t_x)$ and t_x as upper bounds for quantities $s_N[n]$ and t_n, which are otherwise known implicitly for an arbitrary signal. Then, by defining $\xi_n \triangleq \hat{t}_n - \frac{nT}{M}$ and allowing $\Delta_n \triangleq (n - (N-1)M)$, intersection of (2.8) and (2.18) yields that ξ_n is the positive solution to the following equation:

$$\xi_n^2 + \xi_n\left(T_M\Delta_n - \frac{T_M}{2}\right) - \left(\frac{NT_M}{2A\Omega_0} + \frac{T_M^2\Delta_n}{2}\right) = 0$$

17

Finding the discriminant and postulating the positive root yields that ξ_n has the following form:

$$\xi_n = \frac{1}{2} \left[\sqrt{\left(T_M \Delta_n + \frac{T_M}{2}\right)^2 + \frac{2NT_M}{A\Omega_0}} - \left(T_M \Delta_n - \frac{T_M}{2}\right) \right]$$

Then, we can see that $\lim_{n\to\infty} \xi_n = \frac{T_M}{2}$, which would look contradictory without our intuition from comparator construction: From the affine nature of the reference signal and from the fact that $\lim_{t\to\infty} x(t) = 0$, we can see that $\lim_{t\to\infty} r(x(t)) = r(\lim_{t\to\infty} x(t)) = \frac{T_M}{2}$. Therefore, the deviation between uniform sample instances and natural sample instances are absolutely bounded by ξ_n, which converges to $\frac{T_M}{2}$:

$$t_n - \frac{nT}{M} \to \frac{T_M}{2} \tag{2.26}$$

Consequently, we can observe that natural sampling instances and uniform sampling instances do not converge to each other. However, for a given signal, the deviation between natural and uniform sampling instances converges to a finite constant, $\frac{T_M}{2}$, which diminishes with oversampling factor M.

Using the upper bound on the natural sampling instances, we can postulate an upper bound for the natural sample in a sampling interval $t \in [nT_M, (n+1)T_M]$. As Lemma 2.2.3 indicates, that upper bound is $x_N[n] \leq B_r(\hat{t}_n)$. Let,

$$\tilde{\Delta}_n = \Delta_n + \frac{1}{2M} = \left(\frac{n+0.5}{M} - (N-1)\right)$$

With this notational simplicity, the upper bound for natural samples are given as follows:

$$x(t_n) \leq AM \left[\sqrt{\tilde{\Delta}_n^2 + \frac{2N}{AM\pi}} - \tilde{\Delta}_n \right] \tag{2.27}$$

Using Lemma 2.2.3, the upper bound for uniform samples are found from $x\left(\frac{nT}{M}\right) \leq B_r\left(\frac{nT}{M}\right)$, which has the following form:

$$x\left(\frac{nT}{M}\right) \leq \frac{N}{\pi\Delta_n} \tag{2.28}$$

Therefore, for an input signal of the form in (2.14), we can upper-bound the deviation between natural samples and uniform samples as follows:

$$|x_U[n] - x_N[n]| \leq \max \left\{ \left[AM \left(\sqrt{\tilde{\Delta}_n^2 + \frac{2N}{AM\pi}} - \tilde{\Delta}_n \right) - \frac{N}{\pi\Delta_n} \right], AM \left[\sqrt{\tilde{\Delta}_n^2 + \frac{2N}{AM\pi}} - \tilde{\Delta}_n \right] \right\} \tag{2.29}$$

Since Δ_n is a function of n we can see that the natural samples and uniform samples converge to each other with $\mathcal{O}\left(\frac{1}{n}\right)$. In Section 2.3, we justify our results with simulations.

18

2.3   Simulation Results

For our simulations, we have investigated the behavior of natural and uniform samples for the given input model in (2.14) with $N = 10$ degrees of freedom with coefficients c_k chosen symmetrically alternating such that the absolute maximum is achieved as proven in Lemma 2.2.1. We have set the input signal frequency to 10 KHz and traced the signal behavior over 600 cycles. Our simulations focus on demonstration of three fundamental convergence characteristics. First, we observe the energy in the absolute deviation of natural samples from uniform samples in order to observe the effect of the oversampling factor M to propose worst-case deviation scenario for the subsequent simulations. Then, we simulate the worst-case deviation between sampling instances and the corresponding deviation between natural and uniform samples and demonstrate the performance of the proposed upper bounds.

The energy in the absolute deviation function, denoted by E_D is the energy in the signal which is $d[n] \triangleq |x_U[n] - x_N[n]|$ and it depends on the oversampling factor M. Since the input signal is of finite energy and bounded derivative, the following aspects are expected:

1. The energy in the absolute deviation is finite.

2. The energy in the absolute deviation diminishes in the oversampling factor M within a multiplicative constant.

In Chapter 3, we show that the energy of $d[n]$ is given by $E_D = T_M \sum_{n=-\infty}^{\infty} |d[n]|^2$, which we have used to simulate the energy in the deviation function, E_D, and compare it to the uniformly sampled input signal energy, E_X. As (2.29) indicates, in the tail regions, the deviation energy diminishes in $\mathcal{O}\left(\frac{1}{M}\right)$ within a constant factor due to the non-tail region. And Fig. 2.9 illustrates when signal-to-deviation energy (SDR) is defined as $SDR = 10 \log\left(\frac{E_X}{E_D}\right)$, the performance increases in oversampling factor with $\mathcal{O}\left(\log\left(M\right)\right)$. Therefore, the Nyquist sampling case, where $M = 1$ is the worst-case deviation case for lossless natural sampling.

In addition to the choice of c_k maximizing the absolute signal value, we simulate the Nyquist sampling case so that the validity of the bounds are tested for the worst-case deviation. Figure 2.10 indicates that the upper bound in (2.29) captures the convergence characteristics of the natural and uniform samples successfully at the worst-case deviation and illustrate that natural and uniform samples converge in $\mathcal{O}\left(\frac{1}{n}\right)$. For the difference between sampling instances, our simulations justify an important observation, which is the basis of our analysis in Chapter 3; as Fig. 2.11 indicates, the effect of the affine mapping imposed by the reference signal $r(t)$ manifests itself as a difference of $\frac{T}{2M}$ between uniform and natural sampling consistent to (2.21).
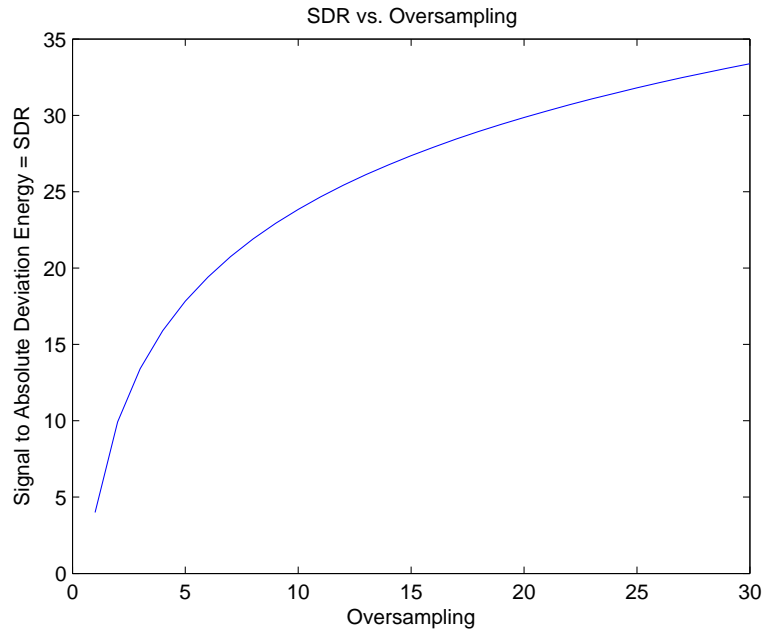
Figure 2.9: Signal to Absolute Deviation Energy vs. Oversampling

The difference between natural samples and uniform samples indicates that for the input signal $x(t) = 0$, the corresponding PWM signal is a 50% duty cycle square wave, which occurs due to the construction of the PWM signal. In the Chapter 3, we motivate this understanding further and propose an approach to isolate this structural component.
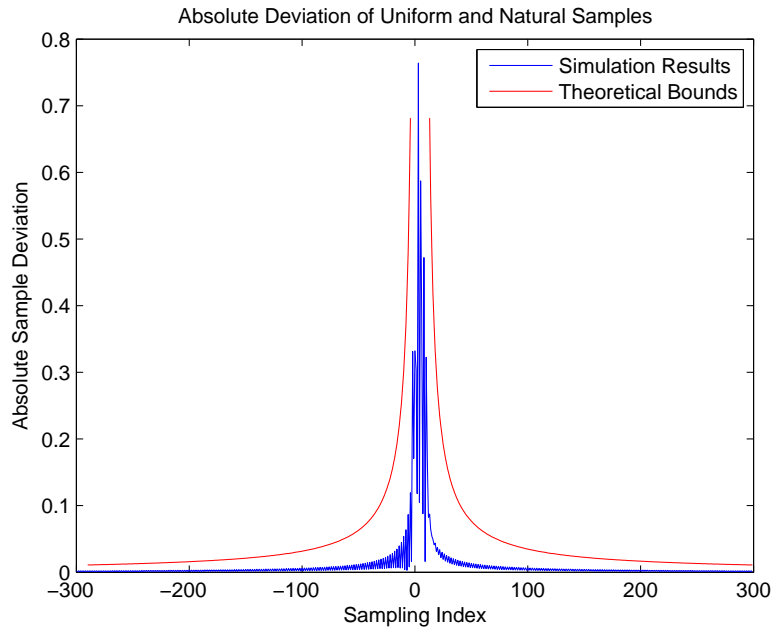
Figure 2.10: Convergence of Natural and Uniform Samples
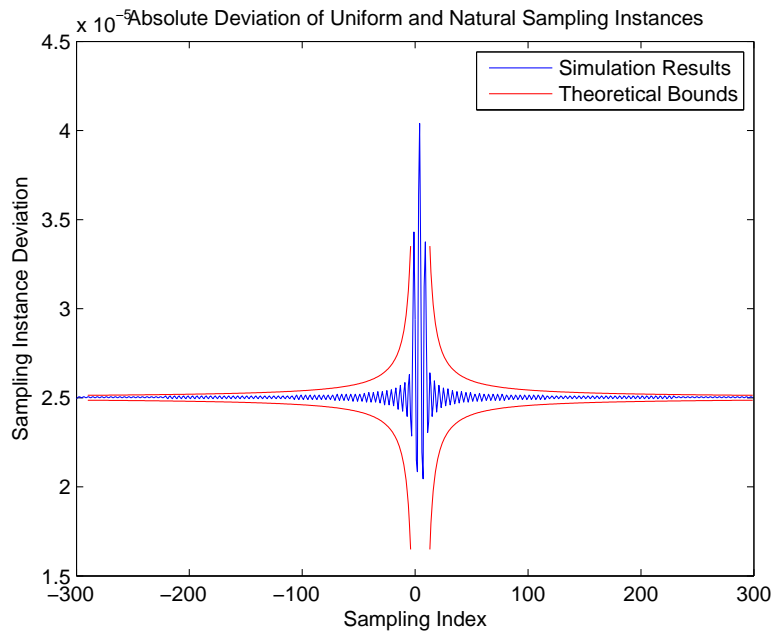
Figure 2.11: Convergence of Natural and Uniform Sampling Instances

Chapter 3

Frequency Domain Analysis

We have shown that a PWM generator can be analyzed in linear blocks and a non-linear block separately. On one hand, the linear blocks consist of the mapping between input samples, x_n, and pulse widths, w_n, and the choice of pulse orientation, which maps w_n to rising and falling edge instances, t_n. On the other hand, the non-linear block is the generation of the PWM signal $p(t)$ from t_n. Even though the comparator construction carries out these operations at once, in analysis, separability of these blocks is preserved in the choice of the reference signal. Furthermore, the sampling methodology changes the sampling instances and sample values, but with a lossless sampling reference signal, perfect reconstruction is possible both natural and uniform sampling, which motivates us to question the availability of a similar separation between linear and non-linear blocks in the reconstruction end. Under the lossless sampling conditions in Theorem 2.1.1, a PWM generator with comparator construction can be treated as a lossless sampler. If the reconstruction mechanism has the information on every instance that the PWM signal changes state, namely the sequence t_n of rising edge and falling edge instances, then, inverse of the affine mapping $f(\cdot)$, which is defined by the PWM generator can be applied to time difference between every consecutive rising edge and falling edge, which results in perfect recovery of the sampled input values. However, such information is not necessarily available in real-life applications, which motivates us to analyze the performance of an alternative reconstruction mechanism. We investigate the performance of continuous time low-pass filtering as a suboptimal, linear reconstruction mechanism for a PWM signal generated from an oversampled input signal. In this chapter, we first introduce a separation principle, where we separate the infinite energy no-information bearing structural component from the finite energy information bearing PWM component, which we name variation signal. Then, we postulate an equivalent model to analyze the low-pass reconstruction from a PWM signal, which involves using the finite energy variation signal instead of the infinite energy PWM signal. Using the equivalent model and frequency domain representation of the information bearing signal component, we derive performance bounds on low-pass reconstruction as a function of the oversampling factor.

3.1 Separation Principle

A PWM generator modifies the input signal by imposing $f(x_n) = w_n$, $\forall n \in \mathbb{Z}$, where $f(\cdot)$ is necessarily an invertible mapping. Thus, an ideal reconstruction mechanism must impose $f^{-1}(\cdot)$ on the output to recover $x(t)$ exactly, which leads to two different interpretations of the PWM generation and reconstruction processes. On one hand, one could consider PWM generation as a sole comparator block, as we discussed in Chapter 2, and apply $f^{-1}(\cdot)$ to the output of the reconstruction. Equivalently, a PWM generator can be modeled as a comparator with a scaled reference signal preceded by $f(\cdot)$ and for low-pass reconstruction, the structural component can be separated from the PWM signal before the reconstruction.

As we have shown in Chapter 2, sampling methodology changes the sampling instances and corresponding samples. However, when lossless sampling conditions are observed, these operations are convergent. As the oversampling factor increases, natural and uniform samples converge to each other, where the deviation between sampling instances converge to fixed constant; $\frac{T_M}{2}$. Therefore, in Chapter 3, we derive the frequency domain representations and low-pass reconstruction characteristics of uniformly sampled PWM signals with different pulse orientations. In other words, we allow (2.7) to define the relation between x_n and w_n explicitly.

The DC component introduced by the mapping in (2.7) manifests itself as an infinite energy structural component in the resulting PWM signal. The structural components for different pulse orientations are given as follows:

$$s_{TE}(t) = \sum_{n=-\infty}^{\infty} u\left(t - nT_M\right) - u\left(t - nT_M - \frac{T_M}{2}\right) \tag{3.1}$$

$$s_{LE}(t) = \sum_{n=-\infty}^{\infty} u\left(t - nT_M + \frac{T_M}{2}\right) - u\left(t - nT_M\right) \tag{3.2}$$

$$s_{DE}(t) = \sum_{n=-\infty}^{\infty} u\left(t - nT_M + \frac{T_M}{4}\right) - u\left(t - nT_M - \frac{T_M}{4}\right) \tag{3.3}$$

A PWM generator as defined in Chapter 2, results in the signal components in (3.1)-(3.3) when the input signal $x(t) = 0$, $\forall t$, therefore, a PWM signal deviates from these signals depending on the input amplitude. Furthermore, for each pulse orientation, signals (3.1)-(3.3), which we denote as $s(t)$ without loss of generality, have the following properties:

1. $s(t)$ is a 50% duty cycle square wave which is of infinite energy.

2. $s(t)$ has harmonic components at $\Omega = 0, \pm M\Omega_0, \pm 3M\Omega_0, \ldots$

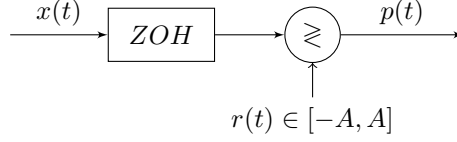3. $s(t)$ is input independent, thus, it is entirely structural.

$x(t)$ → ZOH → $\gtreqless$ → $p(t)$

$r(t) \in [-A, A]$

Figure 3.1: Original Uniformly Sampled PWM Generation

A $\frac{T}{2AM}$

$x(t)$ → $+$ → $\times$ → $w(t)$ → ZOH → $\gtreqless$ → $p(t)$
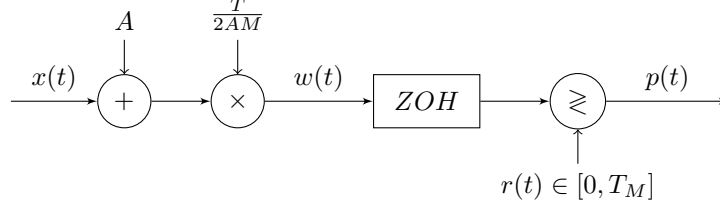
$r(t) \in [0, T_M]$

Figure 3.2: Equivalent Uniformly Sampled PWM Generation

On the generation side, since (2.7) is an affine mapping, a uniformly sampling PWM generator can be modeled either as in Fig. 3.1 or equivalently, as in Fig. 3.2, where the reference signal is scaled to span $[0, T_M]$ instead of $[-A, A]$ since in the equivalent case input of the ZOH block is $w(t) = f(x(t)) \in [0, T_M]$. The equivalent model for the PWM generator follows directly from our discussion Chapter 2.

On the reconstruction side, low-pass filtering is proceeded by $f^{-1}(\cdot)$. For developing an equivalent reconstruction strategy, we first emphasize that continuous-time low-pass filtering is a linear operator, therefore, it is possible to eliminate the DC component in the output before the low-pass filtering by eliminating the signal component corresponding to the DC component in $p(t)$. Our observation on the structural signal component reveals that $s(t)$ is the DC dependent component. Furthermore, only harmonic component of $s(t)$ in the frequency band $[-\Omega_0, \Omega_0]$ is the harmonic at $\Omega = 0$, which is the DC component. Therefore, the linear reconstruction mechanism allows us to construct an equivalent reconstruction mechanism by eliminating $s(t)$ before filtering and changing the scaling factor, consequently, the following two reconstruction mechanisms are equivalent.

1. First, low-pass filter the signal, then apply $f^{-1}(t) = \frac{2Aw(t)}{T_M}w(t) - A$ to the output signal.

2. First, separate the 50% duty cycle square wave, which corresponds to the DC component $\frac{T_M}{2}$, then apply low-pass filter with the gain of $2A$.

Figure 3.3 represents the original reconstruction mechanism and Fig. 3.4 represents the equivalent reconstruction mechanism. The separation approach allows us to manipulate the linear nature of the reconstruction mechanism to isolate the signal dependent component entirely, which has a well-defined frequency domain representation. We allow $v(t) = p(t) - s(t)$, which we name the variation signal, to denote the information bearing part of a PWM signal. Here, $v(t)$ represents the variation of a PWM signal from its
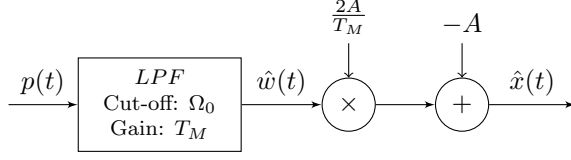
Figure 3.3: Original Input Reconstruction
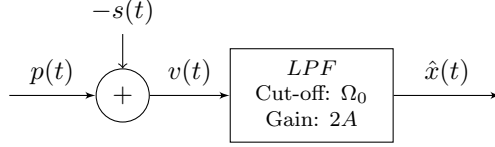
Figure 3.4: Equivalent Input Reconstruction

square wave and it has the following form for fixed-edge PWM signals:

$$v_{TE}(t) = \sum_{n=-\infty}^{\infty} u\left(t - nT_M - \frac{T_M}{2}\right) - u\left(t - nT_M - w_n\right) \tag{3.4}$$

$$v_{LE}(t) = \sum_{n=-\infty}^{\infty} u\left(t - nT_M + w_n\right) - u\left(t - nT_M + \frac{T_M}{2}\right) \tag{3.5}$$

On the other hand, for DEPWM, the variation signal is a sum of trailing-edge and leading-edge components of half width in each symbol interval, which is as follows:

$$v_{DE}(t) = \sum_{n=-\infty}^{\infty} u\left(t - nT_M + \frac{w_n}{2}\right) - u\left(t - nT_M + \frac{T_M}{4}\right) + \sum_{n=-\infty}^{\infty} u\left(t - nT_M - \frac{T_M}{4}\right) - u\left(t - nT_M - \frac{w_n}{2}\right) \tag{3.6}$$

In Section 3.2, we use these signals to derive the frequency domain representation of the signal dependent component of a PWM signal which eventually allows us to formulate performance bounds on low-pass filtering as a suboptimal reconstruction mechanism from PWM signals.

3.2 Frequency Domain Representations of PWM Signals

Variation signals as defined in (3.4)-(3.6) are finite energy signals with pulse energies converging to 0 uniformly, therefore, they have clearly defined frequency domain representations. Allowing $\mathscr{F}\{\cdot\}$ to denote the Fourier transform operator, the frequency domain representation of these information bearing signals are found next. We isolate the band-limited input signal components in the frequency domain of the variation signal, which allows us to evaluate the performance of low-pass filtering. We begin our analysis with fixed-edge PWM constructions.

3.2.1 Frequency Spectra of Fixed-Edge PWM Constructions

For trailing-edge PWM construction, in each symbol interval, the input amplitude information is preserved in the variation from the mid-point $nT_M + \frac{T_M}{2}$. One should emphasize here that even though a variation signal is the only signal-dependent component of a PWM signal, it is not a PWM signal. The frequency domain representation of the variation signal for TEPWM is given as follows:

$$
\begin{aligned}
V_{TE}\left(j\Omega\right) = \mathscr{F}\left\{v_{TE}(t)\right\} &= \int_{-\infty}^{\infty} v_{TE}(t)e^{-j\Omega t}\,dt \\
&= \int_{-\infty}^{\infty}\left[\sum_{n=-\infty}^{\infty} u\left(t - nT_M - \frac{T_M}{2}\right) - u\left(t - nT_M - w_n\right)\right]e^{-j\Omega t}\,dt
\end{aligned}
\tag{3.7}
$$

As $n \to \infty$, the energy of the pulses in the nth symbol interval converges uniformly to 0. Therefore, the order of integration and summation operations can be changed:

$$
V_{TE} = \sum_{n=-\infty}^{\infty}\int_{-\infty}^{\infty}\left[u\left(t - nT_M - \frac{T_M}{2}\right) - u\left(t - nT_M - w_n\right)\right]e^{-j\Omega t}\,dt
$$

Fixing n and passing to the integral limits yield that:

$$
V_{TE}\left(j\Omega\right) = \sum_{n=-\infty}^{\infty}\int_{nT_M+w_n}^{nT_M+\frac{T_M}{2}} e^{-j\Omega t}\,dt = \frac{1}{j\Omega}\sum_{n=-\infty}^{\infty} e^{-j\Omega nT_M}\left[e^{-j\Omega w_n} - e^{-j\Omega\frac{T_M}{2}}\right]
$$

Utilizing (2.7), $V_{TE}(j\Omega)$ reduces to the following:

$$
V_{TE}\left(j\Omega\right) = \frac{T_M}{2A}e^{-j\Omega\frac{T_M}{2}}\sum_{n=-\infty}^{\infty} x_n e^{-j\Omega T_M\left(n+\frac{x_n}{4A}\right)}\operatorname{sinc}\left(\Omega\frac{T_M x_n}{4A}\right)
\tag{3.8}
$$

The complex exponential terms can be rearranged to construct a more intuitive form:

$$
V_{TE}\left(j\Omega\right) = \frac{T_M}{2A}e^{-j\Omega\frac{T_M}{2}}\sum_{n=-\infty}^{\infty} x_n e^{-j\Omega nT_M}\mathscr{C}_n\left(j\Omega\right)
\tag{3.9}
$$

Here, $\mathscr{C}_n\left(j\Omega\right)$ is defined as follows:

$$
\mathscr{C}_n\left(j\Omega\right) = \operatorname{sinc}\left(\Omega\frac{T_M x_n}{4A}\right)e^{-j\Omega\frac{T_M x_n}{4A}}
\tag{3.10}
$$

One should observe that $C(0) = 1$. Therefore, by allowing,

$$
\mathscr{C}_n(j\Omega) = 1 + \mathscr{E}_n(j\Omega)
\tag{3.11}
$$

In $[-\Omega_0, \Omega_0]$, one can utilize Maclaurin series expansion to absolutely upper-bound $\mathscr{E}_n(j\Omega)$, $\forall n \in \mathbb{Z}$. Therefore, the signal-dependent component of a PWM signal can be reduced to the following:

$$V_{TE}(j\Omega) = \frac{T_M}{2A} e^{-j\Omega \frac{T_M}{2}} \sum_{n=-\infty}^{\infty} x_n e^{-j\Omega n T_M} + \frac{T_M}{2A} e^{-j\Omega \frac{T_M}{2}} \sum_{n=-\infty}^{\infty} x_n e^{-j\Omega n T_M} \mathscr{E}_n(j\Omega) \qquad (3.12)$$

TEPWM construction shifts the signal components by $\frac{T_M}{2}$ and the input signal can be recovered from the first component perfectly by low-pass filtering [5]. However, low-pass reconstruction cannot eliminate the signal component that depends on $\mathscr{E}_n(j\Omega)$. Therefore, we refer to the second component as low-pass distortion component. Next, we proceed with the frequency domain analysis of LEPWM, which proves itself to be very similar to that of TEPWM because of their circularly symmetric construction.

Leading-edge PWM construction differs from TEPWM construction by choice of the fixed point in each symbol interval. Thus, the circular symmetry between LEPWM and TEPWM signals leads to change of polarity in shift and the distortion component in the frequency domain. The analysis begins similar to that of TEPWM:

$$\begin{aligned} V_{LE}(j\Omega) &= \int_{-\infty}^{\infty} v_{LE}(t) e^{-j\Omega t}\, dt \\ &= \int_{-\infty}^{\infty} \left[\sum_{n=-\infty}^{\infty} u\left(t - nT_M + w_n\right) - u\left(t - nT_M + \frac{T_M}{2}\right) \right] e^{-j\Omega t}\, dt \end{aligned}$$

The energy in the pulses of $v_{LE}(t)$ converges uniformly to 0, allowing us to change the order of summation and integration:

$$V_{LE}(j\Omega) = \sum_{n=-\infty}^{\infty} \int_{nT_M - \frac{T_M}{2}}^{nT_M - w_n} e^{-j\Omega t}\, dt$$

Rearranging the terms in the same way for that for TEPWM and utilizing (2.7) yield that:

$$V_{LE}(j\Omega) = \frac{T_M}{2A} e^{j\Omega \frac{T_M}{2}} \sum_{n=-\infty}^{\infty} x_n e^{-j\Omega T_M \left(n - \frac{x_n}{4A}\right)} \operatorname{sinc}\left(\Omega \frac{T_M x_n}{4A}\right) \qquad (3.13)$$

Therefore, the circular symmetry between time-domain signals manifests itself as a polarity change in the shift and in the distorting component, yielding $\mathscr{C}_n^*(j\Omega)$ instead of $\mathscr{C}_n(j\Omega)$:

$$V_{LE}(j\Omega) = \frac{T_M}{2A} e^{j\Omega \frac{T_M}{2}} \sum_{n=-\infty}^{\infty} x_n e^{-j\Omega n T_M} \mathscr{C}_n^*(j\Omega) \qquad (3.14)$$

27

Since the conjugation operation preserves the amplitude, we follow our definition in (3.11), which yields that for LEPWM, the input-dependent component can still be isolated:

$$V_{LE}(j\Omega) = \frac{T_M}{2A}e^{j\Omega\frac{T_M}{2}}\sum_{n=-\infty}^{\infty}x_ne^{-j\Omega nT_M} + \frac{T_M}{2A}e^{j\Omega\frac{T_M}{2}}\sum_{n=-\infty}^{\infty}x_ne^{-j\Omega nT_M}\mathscr{E}_n^*(j\Omega) \qquad (3.15)$$

Next, we investigate the frequency domain representation of $v_{DE}(t)$ and observe the main changes, which will lead us to slightly modify our approach in the performance analysis.

3.2.2 Frequency Spectrum of Double-Edge PWM Construction

Different from fixed-edge PWM constructions, the symmetric structure of DEPWM construction allows two information bearing pulses to arise in each symbol interval, one of which is a leading-edge variation signal and the other one is a trailing-edge variation signal. As (3.6) indicates, the leading-edge and trailing-edge pulses never interfere with each other, yielding that the variation signal of a DEPWM signal can be represented as a superposition of leading-edge and trailing-edge components of half widths, which create a distinct frequency domain representation. Since the energy of these pulses converges uniformly to 0 without any overlap, the energy of their sum converges uniformly as well. Therefore, $V_{DE}(j\Omega)$ has the following structure:

$$V_{DE}(j\Omega) = \int_{-\infty}^{\infty}v_{DE}(t)e^{-j\Omega t}\,dt$$

Uniform convergence in pulse energy allows changing the order of summation and integration, then for a fixed n, the pulses may pass to the integration limits, yielding that:

$$V_{DE}(j\Omega) = \sum_{n=-\infty}^{\infty}\int_{nT_M-\frac{w_n}{2}}^{nT_M-\frac{T_M}{4}}e^{-j\Omega t}\,dt + \sum_{n=-\infty}^{\infty}\int_{nT_M+\frac{T_M}{4}}^{nT_M+\frac{w_n}{2}}e^{-j\Omega t}\,dt$$

Therefore, the frequency domain representation of the variation signal of a DEPWM signal is the superposition of frequency domain representations of leading-edge and trailing-edge components, only scaled in frequency:

$$V_{DE}(j\Omega) = \frac{T_M}{4A}e^{-j\Omega\frac{T_M}{4}}\sum_{n=-\infty}^{\infty}x_ne^{-j\Omega nT_M}\mathscr{C}_n\left(j\frac{\Omega}{2}\right) + \frac{T_M}{4A}e^{j\Omega\frac{T_M}{4}}\sum_{n=-\infty}^{\infty}x_ne^{-j\Omega nT_M}\mathscr{C}_n^*\left(j\frac{\Omega}{2}\right) \qquad (3.16)$$

Isolating the common terms allows us to investigate further:

$$V_{DE}(j\Omega) = \frac{T_M}{4A}\sum_{n=-\infty}^{\infty}x_ne^{-j\Omega nT_M}\left[e^{-j\Omega\frac{T_M}{4}}\mathscr{C}_n\left(j\frac{\Omega}{2}\right) + e^{j\Omega\frac{T_M}{4}}\mathscr{C}_n^*\left(j\frac{\Omega}{2}\right)\right]$$

Recalling that $\mathscr{C}_n(\Omega) = 1 + \mathscr{E}_n(\Omega)$, $\forall n$ the summation becomes separable:

$$V_{DE}(j\Omega) = \frac{T_M}{4A} \sum_{n=-\infty}^{\infty} x_n e^{-j\Omega n T_M} \left[e^{-j\Omega \frac{T_M}{4}} + e^{j\Omega \frac{T_M}{4}} \right]$$

$$+ \frac{T_M}{4A} \sum_{n=-\infty}^{\infty} x_n e^{-j\Omega n T_M} \left[e^{-j\Omega \frac{T_M}{4}} \mathscr{E}_n \left(j\frac{\Omega}{2} \right) + e^{j\Omega \frac{T_M}{4}} \mathscr{E}_n^* \left(j\frac{\Omega}{2} \right) \right]$$

Using Euler's formula and collecting complex conjugate terms together provide a more intuitive form:

$$V_{DE}(j\Omega) = \underbrace{\frac{T_M}{2A} \sum_{n=-\infty}^{\infty} x_n e^{-j\Omega n T_M} \cos\left(\frac{\Omega T_M}{4} \right)}_{\text{Blurred signal component}} + \underbrace{\frac{T_M}{2A} \sum_{n=-\infty}^{\infty} x_n e^{-j\Omega n T_M} \mathscr{N}_n(j\Omega)}_{\text{Distortion component}} \qquad (3.17)$$

Here the distorting component now has the following form:

$$\mathscr{N}_n(j\Omega) = \frac{1}{2} \Re \left\{ e^{-j\Omega \frac{T_M}{4}} \mathscr{E}_n \left(j\frac{\Omega}{2} \right) \right\} \qquad (3.18)$$

As (3.17) indicates, DEPWM construction makes the input component in the reconstructed signal blurry, in the sense that when low-pass filtered, the reconstructed signal is shifted forward and backward by $\frac{T_M}{4}$ and normalized. The blurring effect introduces an additional distortion, which we analyze in Section 3.3.

With the frequency domain representation of double-edge PWM signals, we conclude our analysis on the frequency domain representation of PWM signals. One should emphasize that if we were to embrace the impulsive frequency domain representation in this analysis, we would have the harmonic components due to $s(t)$ in the frequency domain representation of $p(t)$, which would only add the DC component in low-pass filtering. In Section 3.3, we investigate the performance of low-pass filtering as a suboptimal reconstruction mechanism.

3.3 Performance of Low-Pass Reconstruction

In this section, we derive the performance bounds on low-pass reconstruction from PWM signals using the reconstruction model in Fig. 3.4, with an ideal low-pass filter as given below:

$$H(j\Omega) = \begin{cases} 2A & \text{if } |\Omega| \leq \Omega_0 \\ 0 & \text{if } |\Omega| > \Omega_0 \end{cases} \qquad (3.19)$$

Equivalently, in this section, we sometimes refer to this filter as $H(j\Omega) = 2A \mathbb{1}\{|\Omega| \leq \Omega_0\}$, which is merely a notational difference. We apply this filter to $v(t)$ to investigate the distortion energy due to

29

low-pass filtering and compare it to the signal energy for different PWM constructions at various levels of oversampling. Allowing $\hat{x}(t)$ to be the reconstructed signal, our objective is to first express $\hat{x}(t)$ in the following form:

$$(v * h)(t) = \hat{x}(t) = x(t) + d(t) \tag{3.20}$$

Here $*$ denotes the convolution operator and $d(t)$ is bounded in energy. Then, we investigate the signal-to-distortion energy as defined below:

$$SDR = \frac{E_X}{E_D} \tag{3.21}$$

The energy in the input signal is denoted by E_X and it is given by $E_X = \int_{-\infty}^{\infty} |x(t)|^2 \, dt$. The same applies for the distortion energy calculations as well. However, we have the frequency domain representation of the reconstructed signal, which includes the frequency domain representation of the sampled signal $x[n] = x(nT_M)$. Therefore, the following form is useful for our energy calculations.

$$E_X = \int_{-\infty}^{\infty} |x(t)|^2 \, dt = T_M \sum_{n=-\infty}^{\infty} |x_n|^2 \tag{3.22}$$

The relation in (3.22) is a well-known result, yet it has significant importance in our analysis. Therefore, we outline the proof.

Proof. We begin with the energy of the continuous-time signal, Rayleigh's identity yields that:

$$\int_{-\infty}^{\infty} |x(t)|^2 \, dt = \frac{1}{2\pi} \int_{-\infty}^{\infty} |X(j\Omega)|^2 \, d\Omega \tag{3.23}$$

Similarly, allowing $\omega = \Omega T_M$, the discrete-time Fourier transform of $x_n = x(nT_M)$ is given as follows:

$$X\left(e^{j\omega}\right) = \sum_{n=-\infty}^{\infty} x[n]e^{-j\omega n} \tag{3.24}$$

Then, the Rayleigh's identity for discrete-time Fourier transform pairs imposes that

$$\sum_{n=-\infty}^{\infty} |x[n]|^2 = \frac{1}{2\pi} \int_{-\pi}^{\pi} \left|X\left(e^{j\omega}\right)\right|^2 \, d\omega \tag{3.25}$$

This allows us to reduce the problem statement into the following:

$$\int_{-\infty}^{\infty} |x(t)|^2 \, dt = T_M \sum_{n=-\infty}^{\infty} |x[n]|^2 \iff \int_{-\infty}^{\infty} |X(j\Omega)|^2 \, d\Omega = T_M \int_{-\pi}^{\pi} \left| X\left(e^{j\omega}\right) \right|^2 \, d\omega \qquad (3.26)$$

Once the sampling period is T_M, we can represent $X(e^{j\omega})$ as follows [5]:

$$X(\omega) = \frac{1}{T_M} \sum_{k=-\infty}^{\infty} X\left(j\frac{\omega}{T_M} - j\frac{2\pi k}{T_M}\right) = \frac{1}{T_M} \sum_{k=-\infty}^{\infty} X\left(j\Omega - j2M\Omega_0 k\right) \qquad (3.27)$$

Then, we proceed with the energy calculations:

$$\int_{-\pi}^{\pi} |X(\omega)|^2 \, d\omega \underset{(1)}{=} \frac{1}{T_M} \int_{-\frac{\pi}{T_M}}^{\frac{\pi}{T_M}} |X(j\Omega T_M)|^2 \, d\Omega \underset{(2)}{=} \frac{1}{T_M} \int_{-M\Omega_0}^{M\Omega_0} |X(j\Omega)|^2 \, d\Omega \underset{(3)}{=} \frac{1}{T_M} \int_{-\Omega_0}^{\Omega_0} |X(j\Omega)|^2 \, d\Omega \qquad (3.28)$$

The first equality follows from change of variables $\omega = \Omega T_M$, the limits in the second equality follow from $\Omega_0 = \frac{\pi}{T}$ and the integral argument follows from (3.27) and the final equality follows from $x(t)$ being band-limited to Ω_0, which concludes our proof. $\square$

Next, we utilize the frequency domain representations of variation signals to derive the performance bounds on the distortion energy for different PWM constructions for various levels of oversampling. Our analysis further reveals fundamental trade-offs between generator complexity and distortion attenuation capacity.

3.3.1 Distortion Energy Bounds for Fixed-Edge PWM Constructions

The frequency domain representation of the variation signals in (3.12) and (3.15) indicate that variation signals for fixed-edge PWM constructions can be represented as a sum of the input component $X\left(e^{j\omega}\right)$ and a low-pass distortion component. Furthermore, (3.9) indicates that fixed-edge PWM constructions introduces a time shift of $\frac{T_M}{2}$. Without loss of generality let us first observe TEPWM. After the delay is eliminated, $\hat{X}(j\Omega)$, the signal reconstructed by the low-pass filter $H(j\Omega) = 2A\mathbb{1}\{|\Omega| \leq \Omega_0\}$, has the following form:

$$\hat{X}_{TE}(j\Omega) = V_{TE}(j\Omega)H(j\Omega)e^{j\Omega\frac{T_M}{2}}$$
$$= \frac{T_M}{2A} \sum_{n=-\infty}^{\infty} x_n e^{-j\Omega n T_M} H(j\Omega) + \frac{T_M}{2A} \sum_{n=-\infty}^{\infty} x_n e^{-j\Omega n T_M} \mathscr{E}_n(j\Omega) H(j\Omega)$$

Since $x(t)$ has bandwidth Ω_0 and it is oversampled, $X(j\Omega) = T_M X\left(e^{j\Omega T_M}\right) \mathbb{1}\left\{|\Omega| \le \Omega_0\right\}$ [5]. Therefore, low-pass filtering yields that:

$$X(j\Omega) = \frac{T_M}{2A} \sum_{n=-\infty}^{\infty} x_n e^{-j\Omega n T_M} H(j\Omega)$$

This allows us to represent the reconstructed signal as the input signal and a distortion component:

$$\hat{X}_{TE}(j\Omega) = X(j\Omega) + D_{TE}(j\Omega)$$

Here, the distortion component for TEPWM, $D_{TE}(j\Omega)$ is defined as:

$$D_{TE}(j\Omega) = \frac{T_M}{2A} \sum_{n=-\infty}^{\infty} x_n e^{-j\Omega n T_M} \mathscr{E}_n(j\Omega) H(j\Omega) \tag{3.29}$$

Allowing that for LEPWM, the shift in the output is eliminated by $\hat{X}_{LE}(j\Omega) = V_{LE}(j\Omega)H(j\Omega)e^{-j\Omega\frac{T_M}{2}}$, low-pass filtering results only in a change of polarity in the distortion component, which is defined as follows:

$$D_{LE}(j\Omega) = \frac{T_M}{2A} \sum_{n=-\infty}^{\infty} x_n e^{-j\Omega n T_M} \mathscr{E}_n^*(j\Omega) H(j\Omega) \tag{3.30}$$

With a well-defined distortion component for low-pass filtering, now we turn our attention to upper-bounding the energy in $D(j\Omega)$:

$$E_D = \frac{1}{2\pi} \int_{-\infty}^{\infty} |D(j\Omega)|^2 \, d\Omega$$

Applying the definition of the low-pass filter $H(j\Omega)$ yields that the distortion energy in the pass band is given as follows:

$$E_D = \frac{1}{2\pi} \int_{-\Omega_0}^{\Omega_0} \left| T_M \sum_{n=-\infty}^{\infty} x_n e^{-j\Omega n T_M} \mathscr{E}_n(j\Omega) \right|^2 \, d\Omega$$

Since $v(t)$ is of finite energy, the argument of the summation converges in energy, which allows us to apply the triangle inequality:

$$E_D \le \frac{1}{2\pi} \int_{-\Omega_0}^{\Omega_0} \left(T_M \sum_{n=-\infty}^{\infty} \left| x_n e^{-j\Omega n T_M} \mathscr{E}_n(j\Omega) \right| \right)^2 \, d\Omega \tag{3.31}$$

At this point, we upper-bound $|\mathscr{E}_n(j\Omega)|$ on $\Omega \in [-\Omega_0, \Omega_0]$, which will allows us to postulate the same distortion bounds for TEPWM and LEPWM since $|\mathscr{E}_n(j\Omega)| = |\mathscr{E}_n^*(j\Omega)|$. First, let us observe the structure

of the distorting component:

$$\mathscr{E}_n(j\Omega) = \text{sinc}\left(\Omega\frac{T_M x_n}{4A}\right)e^{-j\Omega\frac{T_M x_n}{4A}} - 1 \tag{3.32}$$

Therefore, $|\mathscr{E}_n(j\Omega)|$ has the following explicit form:

$$|\mathscr{E}_n(j\Omega)| = \sqrt{\left(\text{sinc}\left(\frac{\Omega T_M x_n}{4A}\right)\right)^2 - 2\,\text{sinc}\left(\frac{\Omega T_M x_n}{2A}\right) + 1} \tag{3.33}$$

Using the Maclaurin series expansion of $|\mathscr{E}_n(j\Omega)|$, we can upper-bound $|\mathscr{E}_n(j\Omega)|$ in $\Omega \in [-\Omega_0, \Omega_0]$:

$$|\mathscr{E}_n(j\Omega)| \leq \left|\frac{\Omega T x_n}{4AM}\right| \tag{3.34}$$

This allows us to upper-bound the energy in the distortion component. The first step is to isolate the input energy term:

$$E_D \leq \frac{1}{2\pi}\int_{-\Omega_0}^{\Omega_0}\left(T_M\sum_{n=-\infty}^{\infty}|x_n|\left|\frac{\Omega T x_n}{4AM}\right|\right)^2 d\Omega = \frac{T^2}{32\pi(AM)^2}\left(T_M\sum_{n=-\infty}^{\infty}|x_n|^2\right)^2\int_{-\Omega_0}^{\Omega_0}\Omega^2\,d\Omega$$

Using (3.22) for E_X yields that the distortion energy diminishes with $\mathcal{O}\left(M^2\right)$:

$$E_D \leq \frac{\pi\Omega_0 E_X^2}{48(AM)^2} \tag{3.35}$$

The corresponding signal-to-distortion ratio is:

$$SDR = \frac{E_X}{E_D} \geq \frac{48(AM)^2}{\pi\Omega_0 E_X} \tag{3.36}$$

We had already shown that since TEPWM and LEPWM signals are circularly symmetric to each other, their frequency domain representations are similar. Now, we have proven that their low-pass reconstruction performances are indeed bounded by identical bounds. Next, we investigate the low-pass reconstruction characteristics of DEPWM signals, which will reveal a fundamental trade-off between generator complexity and distortion attenuation.

3.3.2 Distortion Energy Bound for Double-Edge PWM Construction

Different from the fixed-edge PWM constructions, DEPWM introduces what we call the blurring effect to $X\left(e^{j\Omega T_M}\right)$, which yields an additional distortion component in the output:

$$\hat{X}(j\Omega)_{DE} = V_{DE}(j\Omega)H(j\Omega)$$

$$= X(j\Omega)\cos\left(\frac{\Omega T}{4M}\right) + D_{LP}(j\Omega)$$

Allowing $B(j\Omega) \triangleq \left[\cos\left(\frac{\Omega T}{4M}\right) - 1\right]$ to express the blurring effect, the distortion components can be separated as follows:

$$\hat{X}(j\Omega) = X(j\Omega) + D_B(j\Omega) + D_{LP}(j\Omega) \tag{3.37}$$

The distortion component due to the blurring effect is given by:

$$D_B(j\Omega) = \frac{T_M}{2A}\sum_{n=-\infty}^{\infty} x_n e^{-j\Omega n T_M} B(j\Omega)H(j\Omega) \tag{3.38}$$

The distortion due to low-pass reconstruction is:

$$D_{LP}(j\Omega) = \frac{T_M}{2A}\sum_{n=-\infty}^{\infty} x_n e^{-j\Omega n T_M} \mathscr{N}_n(j\Omega) H(j\Omega) \tag{3.39}$$

Then, the total distortion is $D_{DE}(j\Omega) \triangleq D_B(j\Omega) + D_{LP}(j\Omega)$, where, allowing the distortion energy due to the blurring effect to be E_B and distortion energy due to low-pass filtering to be E_{LP}, the total distortion E_D is bounded as follows [29]:

$$E_D \leq 2\left(E_B + E_{LP}\right) \tag{3.40}$$

Therefore, we first evaluate E_B and E_{LP} separately, then we use (3.40) to upper-bound total distortion energy. We begin with the distortion energy due to blurring:

$$E_B = \frac{1}{2\pi}\int_{-\infty}^{\infty} |D_B(j\Omega)|^2 \, d\Omega = \frac{1}{2\pi}\int_{-\Omega_0}^{\Omega_0} \left|T_M\sum_{n=-\infty}^{\infty} x_n e^{-j\Omega n T_M} B(j\Omega)\right|^2 d\Omega = \frac{1}{2\pi}\int_{-\Omega_0}^{\Omega_0} |X(j\Omega)B(j\Omega)|^2 \, d\Omega$$

Since the integration is on a compact set and $X(j\Omega)$ and $B(j\Omega)$ are both continuous functions, we can upper-bound E_B as follows:

$$E_B \leq \max_{\Omega\in[-\Omega_0,\Omega_0]} |B(j\Omega)|^2 E_X = |B(j\Omega_0)|^2 E_X$$

34

Therefore,

$$E_B \leq \left|1 - \cos\left(\frac{\pi}{4M}\right)\right|^2 E_X \leq \frac{\pi^4}{2^{10} M^4} E_X \tag{3.41}$$

Here the last step follows from the Maclaurin series expansion of $\cos\left(\frac{\pi}{4M}\right)$. The last step clearly emphasizes that the distortion due to the blurring effect diminishes with $\mathcal{O}\left(M^4\right)$. Next, we analyze the distortion energy due to low-pass filtering.

The main distinction between DEPWM construction and the fixed-edge PWM constructions is the attenuation of low-pass reconstruction error, which comes from the bound on the distorting component $\mathcal{N}_n(j\Omega)$. Otherwise, the distortion energy analysis is identical to the TEPWM and LEPWM cases up to equation (3.31). Therefore, we first upper-bound $|\mathcal{N}_n(j\Omega)|$, in the region $\Omega \in [-\Omega_0, \Omega_0]$.

$$\begin{aligned}
|\mathcal{N}_n(j\Omega)| &= \frac{1}{2}\left|\Re\left\{e^{-j\Omega\frac{T_M}{4}} \mathcal{E}_n\left(j\frac{\Omega}{2}\right)\right\}\right| \\
&= \left|\operatorname{sinc}\left(\frac{T_M x_n}{8A}\Omega\right)\cos\left(\left(\frac{T x_n}{8AM} + \frac{T_M}{4}\right)\Omega\right) - \cos\left(\frac{T_M}{4}\Omega\right)\right|
\end{aligned}$$

At this point, the problem is reduced to postulating an upper bound using Maclaurin series expansion with the lowest order of x_n being 1. This is a requirement arising from the fact that $x(t)$ is not necessarily an $\mathscr{L}^1(\mathbb{R})$ signal. Since $\operatorname{sinc}\left(\frac{T_M x_n}{8A}\Omega\right)$ is an even function, in the region $\Omega \in [-\Omega_0, \Omega_0]$, one could observe that $\cos\left(\left(\left|\frac{T_M x_n}{8A}\Omega\right| + \frac{T_M}{4}\right)\Omega\right) \leq \cos\left(\left(\frac{T_M x_n}{8A}\Omega + \frac{T_M}{4}\right)\Omega\right)$, yielding that:

$$|\mathcal{N}_n(j\Omega)| \leq \left|\operatorname{sinc}\left(\left|\frac{T_M x_n}{8A}\right|\Omega\right)\cos\left(\left(\left|\frac{T_M x_n}{8A}\right| + \frac{T_M}{4}\right)\Omega\right) - \cos\left(\frac{T_M}{4}\Omega\right)\right| \tag{3.42}$$

Using Maclaurin series expansion, (3.42) can be reduced to the following polynomial x_n with no constant term, as required:

$$|\mathcal{N}_n(j\Omega)| \leq \Omega^2\left(\frac{2}{3}\left(\frac{T_M x_n}{8A}\right)^2 + \left|\frac{T_M^2 x_n}{32A}\right|\right) \tag{3.43}$$

The rest follows with the same steps as those after (3.31).

$$E_{LP} \leq \frac{\pi^3}{45 \cdot 2^{10}} \frac{\Omega_0(A+3)^2}{(AM)^4} E_X^2 \tag{3.44}$$

Therefore, the total distortion energy is bounded by:

$$E_D \leq \frac{\pi^3}{45 \cdot 2^9} \frac{\Omega_0(A+3)^2}{(AM)^4} E_X^2 + 2\left|1 - \cos\left(\frac{\pi}{4M}\right)\right| E_X \tag{3.45}$$

In a more compact form, we have:

$$E_D \leq \frac{\pi^4}{2^9 M^4} \left[\frac{\Omega_0(A+3)^2}{45\pi A^4} E_X^2 + E_X \right] \tag{3.46}$$

and the corresponding compact signal-to-distortion ratio is given as follows:

$$SDR = \frac{E_X}{E_D} \geq \frac{2^9 M^4}{\pi^4 \left[\frac{\Omega_0(A+3)^2}{45\pi A^4} E_X + 1 \right]} \tag{3.47}$$

Although DEPWM construction introduces a blurring effect, it attenuates the low-pass reconstruction error substantially for high oversampling factors, revealing a trade-off between distortion attenuation and generator complexity.

Chapter 4

Stochastic Analysis

In this chapter, we first postulate a stochastic model of a PWM random process with independent identically distributed (i.i.d.) pulse widths. Then, we observe that due to the affine nature of the PWM generator, one could use the pulse width process as input statistics without loss of information. Following the PWM process model, we show that a PWM process generated from a wide sense stationary (WSS) pulse width process is not necessarily WSS due to the fixed starting point of the PWM process model. Then, by postulating a random starting point on a symbol interval, we show that it is possible to make a PWM process WSS. We finalize this chapter with simulations for different PWM constructions where pulse widths are i.i.d. uniformly distributed.

4.1 Fixed Starting Point Model for PWM Processes

For the stochastic analysis of a PWM signal, first, let a WSS generator process W define i.i.d. pulse widths W_k for the kth pulse of the PWM process P. Under the lossless sampling conditions given in Chapter 2, for any PWM generator, there exists an invertible mapping $f(\cdot)$ between input samples and pulse widths, therefore, the generator process W can be thought as a PWM generator operating over a WSS input process X. Therefore, we can model the input statistics as the pulse width generator process W instead of the input process X, with the understanding that $\forall k$, $\mathbb{P}\{0 \leq W_k < T_M\} = 1$, where T_M is the symbol interval. Then, for given pulse width statistics, PWM processes with different pulse orientations are defined as follows:

$$P_{TE}(t) = \sum_{k=-\infty}^{\infty} \mathbb{1}\{kT_M < t < kT_M + W_k\} \tag{4.1}$$

$$P_{LE}(t) = \sum_{k=-\infty}^{\infty} \mathbb{1}\{kT_M - W_k < t < kT_M\} \tag{4.2}$$

$$P_{DE}(t) = \sum_{k=-\infty}^{\infty} \mathbb{1}\left\{kT_M - \frac{W_k}{2} < t < kT_M + \frac{W_k}{2}\right\} \tag{4.3}$$

Here $\mathbb{1}\{\cdot\}$ denotes the indicator function, thus, P is a continuous time random process for any pulse orientation. One should observe that for any signal structure, there exists a fixed point at each symbol interval. For TEPWM, at $t = kT_M$ there is always a rising edge, for LEPWM at $t = kT_M$, there is always a falling edge and for DEPWM $t = kT_M$ is a fixed point around which, a pulse with random width is oriented. Because of this structure, we name the random processes given in (4.1)-(4.3) as fixed starting point PWM processes, with the understanding that as $W \to 0$, the pulse gets closer to fixed point, thus in that sense, the pulse starts from that fixed point. One should observe that this structure imposes a strict time dependence on the process. Therefore, in this chapter, we show that a PWM process with a fixed starting point is not necessarily WSS. We use the first moment characteristics to observe this behavior. Then, we postulate the additional conditions on the generator process W and show that such conditions would imply a trivial case.

We first postulate modified versions of the complementary cumulative distribution function for notational simplicity. Since $\forall k \in \mathbb{Z}$, $\mathbb{P}\{0 \leq W_k \leq T_M\} = 1$ and W_k are i.i.d., the cumulative distribution function (CDF), $F(t) = \mathbb{P}\{W_k \leq t\}$, has the following properties in addition to its universal properties:

1. $F(t) = 1$, for $t \geq T_M$.

2. $F(t) = 0$, for $t < 0$.

Since the PWM process constructions in (4.1)-(4.3) depend on the complementary CDF of the input statistics, rather than the CDFs themselves, for notational simplicity, we define $\Phi(t) = 1 - F(t))$ and the following modified versions:

$$\hat{\Phi}(t) = \Phi(t)u(t) = \begin{cases} 1 - F(t) & \text{if } t \in [0, T_M] \\ 0 & \text{otherwise} \end{cases} \tag{4.4}$$

$$\check{\Phi}(t) = \hat{\Phi}(-t) \tag{4.5}$$

$$\tilde{\Phi}(t) = \hat{\Phi}(|t|) = \hat{\Phi}(t) + \check{\Phi}(t) \tag{4.6}$$

Here $u(t) = \mathbb{1}\{t \geq 0\}$ is the step function. With this notational simplicity, we now derive the first moments for the given signal constructions, we begin with TEPWM:

$$\mathbb{E}\left[P_{TE}(t)\right] = \mathbb{E}\left[\sum_{k=-\infty}^{\infty} \mathbb{1}\{kT_M < t < kT_M + W_k\}\right]$$

$$= \sum_{k=-\infty}^{\infty} \mathbb{E}\left[\mathbb{1}\{kT_M < t < kT_M + W_k\}\right] = \sum_{k=-\infty}^{\infty} \mathbb{E}\left[\mathbb{1}\{0 < t - kT_M < W_k\}\right] \tag{4.7}$$

The argument of the indicator function has separable impositions, the second of which is deterministic [30]:

$$\mathbb{E}\left[P_{TE}(t)\right] = \sum_{k=-\infty}^{\infty} \mathbb{E}\left[\mathbb{1}\left\{t - kT_M < W_k\right\}\right]\mathbb{1}\left\{t - kT_M > 0\right\}$$

By definition, for and event $\omega \in \Omega$, $\mathbb{E}\left[\mathbb{1}\left\{\omega\right\}\right] = \mathbb{P}\left\{\omega\right\}$:

$$\mathbb{E}\left[P_{TE}(t)\right] = \sum_{k=-\infty}^{\infty} \mathbb{P}\left\{W_k > t - kT_M\right\} = \sum_{k=-\infty}^{\infty} \Phi\left(t - kT_M\right)\mathbb{1}\left\{t - kT_M > 0\right\}$$

which is the definition of $\hat{\Phi}\left(t - kT_M\right)$. Therefore,

$$\mathbb{E}\left[P_{TE}(t)\right] = \sum_{k=-\infty}^{\infty} \hat{\Phi}\left(t - kT_M\right) \tag{4.8}$$

LEPWM and TEPWM are circularly symmetric signals, meaning that in each symbol interval pulses of trailing-edge pulses and leading-edge pulses are reflections of each other with respect to the mid-point of the symbol interval. Therefore, LEPWM has very similar characteristics to those of TEPWM:

$$\mathbb{E}\left[P_{LE}(t)\right] = \mathbb{E}\left[\sum_{k=-\infty}^{\infty} \mathbb{1}\left\{kT_M - W_k < t < kT_M\right\}\right]$$

$$= \sum_{k=-\infty}^{\infty} \mathbb{E}\left[\mathbb{1}\left\{-W_k < t - kT_M < 0\right\}\right]$$

The argument of the indicator function is again separable. Thus,

$$= \sum_{k=-\infty}^{\infty} \mathbb{E}\left[\mathbb{1}\left\{W_k > -(t - kT)\right\}\right]\mathbb{1}\left\{t - kT_M < 0\right\}$$

But, this is the definition of $\hat{\Phi}\left(-(t - kT_M)\right) = \check{\Phi}(t - kT_M)$, yielding that:

$$\mathbb{E}\left[P_{LE}(t)\right] = \sum_{k=-\infty}^{\infty} \check{\Phi}\left(t - kT_M\right) \tag{4.9}$$

On the other hand, for DEPWM, the mid-point of every pulse is fixed, yielding that no rising edge or falling edge is predetermined. Therefore, DEPWM has distinct stochastic characteristics compared to the other PWM structures. The first moment of a fixed starting point DEPWM is as follows:

$$\mathbb{E}\left[P_{DE}(t)\right] = \mathbb{E}\left[\sum_{k=-\infty}^{\infty} \mathbb{1}\left\{kT_M - \frac{W_k}{2} < t < kT_M + \frac{W_k}{2}\right\}\right]$$

$$= \sum_{k=-\infty}^{\infty} \mathbb{P}\left\{-\frac{W_k}{2} < t - kT_M < \frac{W_k}{2}\right\} = \sum_{k=-\infty}^{\infty} \mathbb{P}\left\{|t - kT_M| < \frac{W_k}{2}\right\}$$

Since $\forall k$, $\mathbb{P}\left\{0 \leq W_k < T_M\right\} = 1$, by the definition of $\tilde{\Phi}(t)$, the rest follows:

$$\mathbb{E}\left[P_{DE}(t)\right] = \sum_{k=-\infty}^{\infty} \tilde{\Phi}\left(2(t - kT_M)\right) \tag{4.10}$$

As (4.1)-(4.3) indicate, the first moments of the fixed starting point PWM processes as defined in (4.1)-(4.3) depend on t. Therefore, a PWM process with a fixed starting point is not necessarily WSS. For intuition,

we inspect a case where the first moments are necessarily constant in time. That is, when $\Phi(t) = 1$, $\forall t < T_M$, which is the trivial case where $\mathbb{P}\{W_k = 0\} = 1$, $\forall k$. Therefore, we conclude that a PWM process with a fixed starting point is not WSS. In Section 4.2, we introduce a randomized starting point over a symbol interval and show that by introducing a randomized starting point the PWM process can be made PWM.

4.2 Randomized Starting Point Model for PWM Processes

In this section, we introduce a randomized starting point $\Theta = \theta$, where $\Theta \sim \text{Unif}[0, T_M]$ in order to eliminate the time dependence due to the pulse constructions given in (4.1)-(4.3). Then, the randomized starting point model for a PWM signal is then given as follows:

$$P_{TE}(t; \theta) = \sum_{k=-\infty}^{\infty} \mathbb{1}\{kT_M < t - \theta < kT_M + W_k\} \tag{4.11}$$

$$P_{LE}(t; \theta) = \sum_{k=-\infty}^{\infty} \mathbb{1}\{kT_M - W_k < t - \theta < kT_M\} \tag{4.12}$$

$$P_{DE}(t; \theta) = \sum_{k=-\infty}^{\infty} \mathbb{1}\left\{kT_M - \frac{W_k}{2} < t - \theta < kT_M + \frac{W_k}{2}\right\} \tag{4.13}$$

With the signal definitions in (4.11)-(4.13), we now show that a PWM process with a randomized starting point is necessarily WSS. Then, we make observations on the stochastic characteristics of different PWM constructions. However, we should make an important observation before the calculation of moments: Θ and W are independent of each other. In other words, a PWM generator does not impose a randomized starting point, but in order to eliminate the time dependence due to the definition of the PWM signal, we should introduce a randomized starting point.

With this remark in mind, we start our derivations for the first moments of the PWM processes with randomized starting points. We again begin with TEPWM:

$$\mathbb{E}\left[P_{TE}(t; \theta)\right] = \mathbb{E}_\theta\left[\mathbb{E}_{W|\theta}\left[P_{TE}(t; \theta)\right]\right] = \mathbb{E}_\theta\left[\mathbb{E}_{W|\theta}\left[\sum_{k=-\infty}^{\infty} \mathbb{1}\{kT_M < t - \theta < kT_M + W_k\}\right]\right]$$

where the first equality follows from the independence of Θ and W and for a fixed θ:

$$\mathbb{E}\left[P_{TE}(t; \theta)\right] = \mathbb{E}_\theta\left[\sum_{k=-\infty}^{\infty} \mathbb{P}_{W|\theta}\{kT_M < t - \theta < kT_M + W_k\}\right]$$

Following the derivation for the first moments for the fixed starting point model, we can observe that:

$$\mathbb{E}\left[P_{TE}(t; \theta)\right] = \mathbb{E}_\theta\left[\sum_{k=-\infty}^{\infty} \hat{\Phi}\left(t - \theta - kT_M\right)\right] \tag{4.14}$$

By the definition of expectation operator,

$$\mathbb{E}\left[P_{TE}(t;\theta)\right] = \int_{-\infty}^{\infty} f_{\Theta}(\theta) \sum_{k=-\infty}^{\infty} \hat{\Phi}\left(t - kT_M - \theta\right) d\theta$$

Since $\Theta \sim \text{Unif}[0, T_M]$:

$$\mathbb{E}\left[P_{TE}(t;\theta)\right] = \int_{0}^{T_M} \frac{1}{T_M} \sum_{k=-\infty}^{\infty} \hat{\Phi}\left(t - \theta - kT_M\right) d\theta$$

For a fixed k, we can change the variable of integration by $\beta = t - \theta - kT_M$. Then,

$$\mathbb{E}\left[P_{TE}(t;\theta)\right] = \frac{1}{T_M} \sum_{k=-\infty}^{\infty} \int_{t-(k-1)T_M}^{t-kT_M} \hat{\Phi}\left(\beta\right) d\beta$$

Therefore,

$$\mathbb{E}\left[P_{TE}(t;\theta)\right] = \frac{1}{T_M} \int_{-\infty}^{\infty} \hat{\Phi}\left(\beta\right) d\beta \tag{4.15}$$

Since TEPWM and LEPWM are circularly symmetric, derivation for the first moment of the LEPWM is very similar to that of the TEPWM.

$$\mathbb{E}\left[P_{LE}(t;\theta)\right] = \mathbb{E}_{\theta}\left[\mathbb{E}_{W|\theta}\left[P_{LE}(t;\theta)\right]\right] = \mathbb{E}_{\theta}\left[\mathbb{E}_{W|\theta}\left[\sum_{k=-\infty}^{\infty} \mathbb{1}\left\{kT_M - W_k < t - \theta < kT_M\right\}\right]\right]$$

Following the same steps as those for (4.14) yields that:

$$= \mathbb{E}_{\theta}\left[\sum_{k=-\infty}^{\infty} \check{\Phi}\left(t - \theta - kT_M\right)\right]$$

Then, applying the change of variables $\beta = t - \theta - kT_M$ leads to a similar sum of integrals except for the argument of the integration:

$$= \frac{1}{T_M} \sum_{k=-\infty}^{\infty} \int_{t-(k-1)T_M}^{t-kT_M} \check{\Phi}\left(\beta\right) d\beta = \frac{1}{T_M} \int_{-\infty}^{\infty} \check{\Phi}\left(\beta\right) d\beta$$

Since $\hat{\Phi}(t) = \check{\Phi}(-t)$, the integration yields the same expectation as that for TEPWM:

$$\mathbb{E}\left[P_{LE}(t;\theta)\right] = \frac{1}{T_M} \int_{-\infty}^{\infty} \hat{\Phi}\left(\beta\right) d\beta \tag{4.16}$$

The first moment calculations for the DEPWM differs slightly from the previous PWM constructions. The derivation is as follows:

$$\mathbb{E}\left[P_{DE}(t;\theta)\right] = \mathbb{E}_{\theta}\left[\mathbb{E}_{W|\theta}\left[P_{DE}(t;\theta)\right]\right] = \mathbb{E}_{\theta}\left[\mathbb{E}_{W|\theta}\left[\sum_{k=-\infty}^{\infty} \mathbb{1}\left\{kT_M - \frac{W_k}{2} < t - \theta < kT_M + \frac{W_k}{2}\right\}\right]\right]$$

Following the same steps as those for (4.14) yields that:

$$= \mathbb{E}_{\theta}\left[\sum_{k=-\infty}^{\infty} \tilde{\Phi}\left(2(t - \theta - kT_M)\right)\right]$$

Allowing change of variables $\beta = 2(t - \theta - kT_M)$ for the expectation integral yields that:

$$\mathbb{E}\left[P_{DE}(t;\theta)\right] = \frac{1}{2T_M} \int_{-\infty}^{\infty} \tilde{\Phi}(\beta) \; d\beta \tag{4.17}$$

This satisfies the finite first moment requirement for the randomized starting point PWM processes to be WSS and motivates us to derive the second moments of the randomized starting point PWM processes. The autocorrelation functions are formulated as follows:

$$R_P(t,s) = \mathbb{E}_\theta\left[\mathbb{E}_{W|\theta}\left[P(t;\theta)P(s;\theta)\right]\right] \tag{4.18}$$

We will first outline the mechanics behind the second moment calculations. For each PWM construction, we first use the fact that W_k are i.i.d. to separate the variation terms and correlation terms. For the correlation terms, since W_k are i.i.d., we separate the terms depending on the different pulse widths and apply a change of variables twice to reduce the θ-expectation to an intuitive form. Then, we show that the variation terms depend on the comparison of given two time instants, which reduces to a function of the difference between those instances. We begin our derivation with the TEPWM case:

$$R_{P_{TE}}(t,s) = \mathbb{E}_\theta\left[\mathbb{E}_{W|\theta}\left[\sum_{k=-\infty}^{\infty} \mathbb{1}\left\{kT_M < t - \theta < kT_M + W_k\right\} \sum_{l=-\infty}^{\infty} \mathbb{1}\left\{lT_M < s - \theta < lT_M + W_l\right\}\right]\right]$$

Changing the order of the linear operations, we impose $\mathbb{E}_{W|\theta}[\cdot]$ first:

$$= \mathbb{E}_\theta\left[\sum_{k=-\infty}^{\infty}\sum_{l=-\infty}^{\infty} \mathbb{E}_{W|\theta}\left[\mathbb{1}\left\{W_k > (t - kT_M - \theta) > 0\right\}\mathbb{1}\left\{W_l > (s - lT_M - \theta) > 0\right\}\right]\right]$$

At this point, we separate the correlation and variation terms in the argument of $\mathbb{E}_{W|\theta}[\cdot]$.

$$R_{P_{TE}}(t,s) = \mathbb{E}_\theta\left[\underbrace{\sum_{\substack{k=-\infty\\k\neq l}}^{\infty}\sum_{k=-\infty}^{\infty} \underbrace{\mathbb{E}_{W|\theta}\left[\mathbb{1}\left\{W_k > (t - kT_M - \theta) > 0\right\}\mathbb{1}\left\{W_l > (s - lT_M - \theta) > 0\right\}\right]}_{S_c(k,l)}}_{\text{Correlation Terms}}\right] \tag{4.19}$$

$$+ \mathbb{E}_\theta\left[\underbrace{\sum_{\substack{k=-\infty\\k=l}}^{\infty}\sum_{l=-\infty}^{\infty} \underbrace{\mathbb{E}_{W|\theta}\left[\mathbb{1}\left\{W_k > (t - kT_M - \theta) > 0\right\}\mathbb{1}\left\{W_l > (s - lT_M - \theta) > 0\right\}\right]}_{S_v(k,l)=S_v(k)=S_v(l)}}_{\text{Variation Terms}}\right] \tag{4.20}$$

Now, we analyze the correlation terms in (4.19) and the variation terms in (4.20) separately. We begin with an observation, since W_k are i.i.d., the argument of summation in (4.19), which we denote as $S_c(k,l)$

reduces to the following:

$$S_c(k,l) = \mathbb{E}_{W|\theta} \left[\mathbb{1}\left\{ W_k > (t - kT_M - \theta) > 0 \right\} \mathbb{1}\left\{ W_l > (s - lT_M - \theta) > 0 \right\} \right]$$

$$= \mathbb{E}_{W|\theta} \left[\mathbb{1}\left\{ W_k > (t - kT_M - \theta) > 0 \right\} \right] \mathbb{E}_{W|\theta} \left[\mathbb{1}\left\{ W_l > (s - lT_M - \theta) > 0 \right\} \right]$$

Since $\mathbb{E}_{W|\theta}[\omega] = \mathbb{P}_{W|\theta}[\omega]$, $\forall \omega \in \Omega$:

$$= \mathbb{P}_{W|\theta} \left[\mathbb{1}\left\{ W_k > (t - kT_M - \theta) > 0 \right\} \right] \mathbb{P}_{W|\theta} \left[\mathbb{1}\left\{ W_l > (s - lT_M - \theta) > 0 \right\} \right]$$

But, these terms have already been computed for the first moment calculations in (4.8) and (4.14). Therefore, the argument of summation reduces to the following:

$$S_c(k,l) = \hat{\Phi}\left(t - kT_M - \theta\right) \hat{\Phi}\left(s - lT_M - \theta\right) \tag{4.21}$$

To avoid confusion, we emphasize that (4.21) is the argument of the correlation sum, which holds only for $k \neq l$. We continue formulating the correlation terms, which are given as follows:

$$\mathbb{E}_\theta \left[\sum_{\substack{k=-\infty \\ k \neq l}}^{\infty} \sum_{l=-\infty}^{\infty} S_c(k,l) \right] = \mathbb{E}_\theta \left[\sum_{\substack{k=-\infty \\ k \neq l}}^{\infty} \sum_{l=-\infty}^{\infty} \hat{\Phi}\left(t - kT_M - \theta\right) \hat{\Phi}\left(s - lT_M - \theta\right) \right]$$

Changing the order of the linear operations, we impose $\mathbb{E}_\theta[\cdot]$ first:

$$= \sum_{\substack{k=-\infty \\ k \neq l}}^{\infty} \sum_{l=-\infty}^{\infty} \mathbb{E}_\theta \left[\hat{\Phi}\left(t - kT_M - \theta\right) \hat{\Phi}\left(s - lT_M - \theta\right) \right]$$

Changing the order of summation, since $\Theta \sim \mathrm{Unif}[0, T_M]$:

$$= \sum_{\substack{l=-\infty \\ k \neq l}}^{\infty} \sum_{k=-\infty}^{\infty} \int_0^{T_M} \frac{1}{T_M} \hat{\Phi}\left(t - kT_M - \theta\right) \hat{\Phi}\left(s - lT_M - \theta\right) d\theta$$

At this point, we postulate a series of meticulous change of variables. We begin with fixing l and proposing the change of variables by $\alpha = \theta - (s - lT_M)$:

$$\mathbb{E}_\theta \left[\sum_{\substack{k=-\infty \\ k \neq l}}^{\infty} \sum_{l=-\infty}^{\infty} S_c(k,l) \right] = \frac{1}{T_M} \sum_{\substack{l=-\infty \\ k \neq l, \text{ fixed } l}}^{\infty} \sum_{k=-\infty}^{\infty} \int_{-(s-lT_M)}^{T_M - (s-lT_M)} \hat{\Phi}\left(\underbrace{t-s}_{\tau} - \underbrace{(k-l)}_{n} T_M - \alpha \right) \hat{\Phi}\left(-\alpha\right) d\alpha$$

Allowing $\tau = t - s$ and $n = k - l$, the expression reduces to the following:

$$= \frac{1}{T_M} \sum_{l=-\infty}^{\infty} \sum_{\substack{n=k-l \\ n=-\infty \\ k \neq l \Rightarrow n \neq 0}}^{\infty} \int_{-(s-lT_M)}^{T - (s-lT_M)} \hat{\Phi}\left(\tau - nT_M - \alpha\right) \hat{\Phi}\left(-\alpha\right) d\alpha$$

Since l was fixed, we can change the order of summation again:

$$= \frac{1}{T_M} \sum_{\substack{n=-\infty \\ n \neq 0}}^{\infty} \sum_{l=-\infty}^{\infty} \int_{-(s-lT_M)}^{T_M - (s-lT_M)} \hat{\Phi}\left(\tau - nT_M - \alpha\right) \hat{\Phi}\left(-\alpha\right) d\alpha$$

The summation of integrations over any given symbol interval spans the entire real axis, yielding that:

$$\mathbb{E}_\theta \left[\sum_{\substack{k=-\infty \\ k \neq l}}^{\infty} \sum_{l=-\infty}^{\infty} S_c(k,l) \right] = \frac{1}{T_M} \sum_{\substack{n=-\infty \\ n \neq 0}}^{\infty} \int_{-\infty}^{\infty} \hat{\Phi}\left(\tau - nT_M - \alpha\right) \hat{\Phi}\left(-\alpha\right) d\alpha \tag{4.22}$$

Since $\hat{\Phi}(t) = \check{\Phi}(-t)$:

$$= \frac{1}{T_M} \sum_{\substack{n=-\infty \\ n \neq 0}}^{\infty} \int_{-\infty}^{\infty} \hat{\Phi}\left(\tau - nT_M - \alpha\right) \check{\Phi}\left(\alpha\right) d\alpha$$

We can observe that the argument of summation is a convolution integral where the convolution operation ($*$) on functions $f(\tau)$ and $g(\tau)$ is defined as follows:

$$(f * g)(\tau) \triangleq \int_{-\infty}^{\infty} f(\beta) g(\tau - \beta) \, d\beta \tag{4.23}$$

Therefore, the correlation terms of for the autocorrelation function of a TEPWM process reduce to the following form:

$$\mathbb{E}_\theta \left[\sum_{\substack{k=-\infty \\ k \neq l}}^{\infty} \sum_{k=-\infty}^{\infty} S_c(k,l) \right] = \frac{1}{T_M} \sum_{\substack{n=-\infty \\ n \neq 0}}^{\infty} \left(\hat{\Phi} * \check{\Phi} \right)(\tau - nT_M) \tag{4.24}$$

Now, we turn our attention to the variation terms, which we denote by $S_v(k,l)$. Since $k = l$, $S_v(k,l)$ is a function of $n = k = l$ only and it has the following form:

$$S_v(k,l) = \mathbb{E}_{W|\theta} \left[\mathbb{1}\left\{ W_k > (t - kT_M - \theta) > 0 \right\} \mathbb{1}\left\{ W_l > (s - lT_M - \theta) > 0 \right\} \right]$$

Since $n = k = l$,

$$S_v(k,l) = S_v(n) = \mathbb{E}_{W|\theta} \left[\mathbb{1}\left\{ W_n > (t - nT_M - \theta) > 0 \right\} \mathbb{1}\left\{ W_n > (s - nT_M - \theta) > 0 \right\} \right]$$

As we have encountered previously, the indicator functions have separable impositions:

$$S_v(n) = \mathbb{E}_{W|\theta} \left[\mathbb{1}\left\{ W_n > (t - nT_M - \theta) \right\} \mathbb{1}\left\{ W_n > (s - nT_M - \theta) \right\} \right]$$

$$\times \mathbb{1}\left\{ (t - nT_M - \theta) > 0 \right\} \mathbb{1}\left\{ (s - nT_M - \theta) > 0 \right\}$$

There are two indicator operations on the random variable W_n and there are two additional deterministic conditions. Gathering these conditions together yields the following:

$$S_v(n) = \mathbb{E}_{W|\theta} \left[\mathbb{1}\left\{ W_n > \max\left\{ (t - nT_M - \theta), (s - nT_M - \theta) \right\} \right\} \right] \mathbb{1}\left\{ \min\left\{ (t - nT_M - \theta), (s - nT_M - \theta) \right\} > 0 \right\}$$

$$= \mathbb{P}_{W|\theta} \left\{ W_n > \max\left\{ (t - nT_M - \theta), (s - nT_M - \theta) \right\} \right\} \mathbb{1}\left\{ \min\left\{ (t - nT_M - \theta), (s - nT_M - \theta) \right\} > 0 \right\}$$

By the definition of the complementary CDF, $\Phi(t)$, this expression further reduces:

$$S_v(n) = \Phi\left(\max\left\{ (t - nT_M - \theta), (s - nT_M - \theta) \right\} \right) \mathbb{1}\left\{ \min\left\{ (t - nT_M - \theta), (s - nT_M - \theta) \right\} > 0 \right\} \tag{4.25}$$

With the structure given in (4.25), we can formulate the variation terms for the autocorrelation function of a TEPWM process:

$$\mathbb{E}_\theta \left[\sum_{n=-\infty}^{\infty} S_v(n) \right] =$$

$$= \mathbb{E}_\theta \left[\sum_{n=-\infty}^{\infty} \Phi \left(\max \left\{ (t - nT_M - \theta), (s - nT_M - \theta) \right\} \right) \mathbb{1} \left\{ \min \left\{ (t - nT_M - \theta), (s - nT_M - \theta) \right\} > 0 \right\} \right]$$

Changing the order of the linear operations, we impose the expectation first:

$$= \sum_{n=-\infty}^{\infty} \int_0^{T_M} \frac{1}{T_M} \Phi \left(\max \left\{ (t - nT_M - \theta), (s - nT_M - \theta) \right\} \right) \mathbb{1} \left\{ \min \left\{ (t - nT_M - \theta), (s - nT_M - \theta) \right\} > 0 \right\} d\theta$$

For a fixed n, proposing the change of variables, $\theta = \gamma + s - nT_M$ yields that:

$$= \frac{1}{T_M} \sum_{n=-\infty}^{\infty} \int_{-(s-nT_M)}^{-(s-(n+1)T_M)} \Phi \left(\max \left\{ (t - s - \gamma), (-\gamma) \right\} \right) \mathbb{1} \left\{ \min \left\{ (t - s - \gamma), (-\gamma) \right\} > 0 \right\} d\gamma$$

Following the definition $\tau = t - s$, the summation of integrations over every given symbol interval spans the entire time axis. Therefore,

$$\mathbb{E}_\theta \left[\sum_{n=-\infty}^{\infty} S_v(n) \right] = \frac{1}{T_M} \int_{-\infty}^{\infty} \Phi \left(\max \left\{ (\tau - \gamma), (-\gamma) \right\} \right) \mathbb{1} \left\{ \min \left\{ (\tau - \gamma), (-\gamma) \right\} > 0 \right\} d\gamma$$

$$= \frac{1}{T_M} \int_{-\infty}^{\infty} \Phi \left(\max \left\{ \tau, 0 \right\} - \gamma \right) \mathbb{1} \left\{ \min \left\{ \tau, 0 \right\} > \gamma \right\} d\gamma \tag{4.26}$$

The expression in (4.26) can be evaluated in two different cases:

1. Let $\tau > 0$. Then, $\max \left\{ \tau, 0 \right\} = \tau$ and $\min \left\{ \tau, 0 \right\} = 0$, which yields that:

$$\mathbb{E}_\theta \left[\sum_{n=-\infty}^{\infty} S_v(n) \right] = \frac{1}{T_M} \int_{-\infty}^{\infty} \Phi (\tau - \gamma) \mathbb{1} \left\{ \gamma < 0 \right\} d\gamma = \frac{1}{T_M} \int_{-\infty}^{0} \Phi (\tau - \gamma) d\gamma \tag{4.27}$$

2. Let $\tau < 0$. Then, $\max \left\{ \tau, 0 \right\} = 0$ and $\min \left\{ \tau, 0 \right\} = \tau$, which yields that:

$$\mathbb{E}_\theta \left[\sum_{n=-\infty}^{\infty} S_v(n) \right] = \frac{1}{T_M} \int_{-\infty}^{\infty} \Phi (-\gamma) \mathbb{1} \left\{ \gamma < \tau \right\} d\gamma = \frac{1}{T_M} \int_{-\infty}^{\tau} \Phi (-\gamma) d\gamma$$

By introducing a change of variables, $\alpha = \gamma - \tau$, we can construct a more intuitive form:

$$= \frac{1}{T_M} \int_{-\infty}^{0} \Phi (-\tau - \alpha) d\alpha \tag{4.28}$$

45

As the cases above indicate, (4.26) equals (4.27) of $\tau > 0$ and it equals (4.28). Therefore, we can collect these two cases into one form:

$$\mathbb{E}_\theta \left[\sum_{n=-\infty}^\infty S_v(n) \right] = \frac{1}{T_M} \int_{-\infty}^0 \Phi\left(|\tau| - \gamma\right) d\gamma = \frac{1}{T_M} \int_{|\tau|}^\infty \Phi(\alpha) \, d\alpha \tag{4.29}$$

Gathering the correlation terms in (4.24) and the variation terms in (4.29) yields in the autocorrelation function of a randomized starting point TEPWM process, which is given as follows:

$$R_{P_{TE}}(\tau) = \frac{1}{T_M} \left[\sum_{\substack{n=-\infty \\ n \neq 0}}^\infty \left(\hat{\Phi} * \check{\Phi}\right)(\tau - nT_M) + \int_{|\tau|}^\infty \Phi(\alpha) \, d\alpha \right] \tag{4.30}$$

For a randomized starting point LEPWM process, the second moment characteristics are identical to those of TEPWM and the mechanics for computing the second moment of LEPWM is very similar to those for TEPWM. Therefore, we merely emphasize the differences between the steps for computing the second moment of LEPWM and those for TEPWM. We begin with the separation of variance and correlation terms:

$$R_{P_{LE}}(t,s) = \mathbb{E}_\theta \left[\mathbb{E}_{W|\theta} \left[\sum_{k=-\infty}^\infty \mathbb{1}\left\{kT_M - W_k < t - \theta < kT_M\right\} \sum_{l=-\infty}^\infty \mathbb{1}\left\{lT_M - W_l < s - \theta < lT_M\right\} \right] \right]$$

$$= \mathbb{E}_\theta \left[\sum_{\substack{k=-\infty \\ k \neq l}}^\infty \sum_{l=-\infty}^\infty S_c(k,l) \right] + \mathbb{E}_\theta \left[\sum_{n=-\infty}^\infty S_v(n) \right]$$

With the understanding that for LEPWM:

$$S_c(k,l) = \mathbb{E}_{W|\theta} \left[\mathbb{1}\left\{W_k > -(t - kT_M - \theta) > 0\right\} \mathbb{1}\left\{W_l > -(s - lT_M - \theta) > 0\right\} \right] \tag{4.31}$$

$$S_v(n) = \mathbb{E}_{W|\theta} \left[\mathbb{1}\left\{W_n > -(t - nT_M - \theta) > 0\right\} \mathbb{1}\left\{W_n > -(s - nT_M - \theta) > 0\right\} \right] \tag{4.32}$$

Since W_k are i.i.d. for $k \neq l$, the correlation terms in (4.31) are in the following form:

$$S_c(k,l) = \check{\Phi}\left(t - kT_M - \theta\right) \check{\Phi}\left(s - lT_M - \theta\right)$$

Then, following exactly the same steps between (4.21) and (4.22) yields that:

$$\mathbb{E}_\theta \left[\sum_{\substack{k=-\infty \\ k \neq l}}^\infty \sum_{l=-\infty}^\infty S_c(k,l) \right] = \frac{1}{T_M} \sum_{\substack{n=-\infty \\ n \neq 0}}^\infty \int_{-\infty}^\infty \check{\Phi}\left(\tau - nT_M - \alpha\right) \check{\Phi}\left(-\alpha\right) d\alpha \tag{4.33}$$

Since $\hat{\Phi}(t) = \check{\Phi}(-t)$, we can postulate a convolution intergral form:

$$= \frac{1}{T_M} \sum_{\substack{n=-\infty \\ n \neq 0}}^{\infty} \int_{-\infty}^{\infty} \check{\Phi}\left(\tau - nT_M - \alpha\right) \hat{\Phi}\left(\alpha\right) \, d\alpha$$

Since convolution is a symmetric operator, the correlation terms for TEPWM and LEPWM processes have the same structure, as given below:

$$\mathbb{E}_\theta \left[\sum_{\substack{k=-\infty \\ k \neq l}}^{\infty} \sum_{l=-\infty}^{\infty} S_c(k,l) \right] = \frac{1}{T_M} \sum_{\substack{n=-\infty \\ n \neq 0}}^{\infty} \left(\check{\Phi} * \hat{\Phi} \right)\left(\tau - nT_M\right) \tag{4.34}$$

The computation of variation terms are similar to what we have done for the TEPWM case. We begin with a separation of impositions:

$$S_v(n) = \mathbb{E}_{W|\theta}\left[\mathbb{1}\left\{W_n > -\left(t - nT_M - \theta\right)\right\} \mathbb{1}\left\{W_n > -\left(s - nT_M - \theta\right)\right\} \right]$$

$$\times \, \mathbb{1}\left\{\left(t - nT_M - \theta\right) < 0\right\} \mathbb{1}\left\{\left(s - nT_M - \theta\right) < 0\right\}$$

As one could expect, the reversed polarity in the rising and falling edge instances of the LEPWM process with respect to the TEPWM process, results in a different form than that in (4.25):

$$S_v(n) = \mathbb{P}_{W|\theta}\left\{W_n > \max\left\{-\left(t - nT_M - \theta\right), -\left(s - nT_M - \theta\right)\right\}\right\} \mathbb{1}\left\{\max\left\{\left(t - nT_M - \theta\right), \left(s - nT_M - \theta\right)\right\} < 0\right\}$$

$$= \mathbb{P}_{W|\theta}\left\{W_n > -\min\left\{\left(t - nT_M - \theta\right), \left(s - nT_M - \theta\right)\right\}\right\} \mathbb{1}\left\{\max\left\{\left(t - nT_M - \theta\right), \left(s - nT_M - \theta\right)\right\} < 0\right\}$$

$$S_v(n) = \Phi\left(-\min\left\{\left(t - nT_M - \theta\right), \left(s - nT_M - \theta\right)\right\}\right) \mathbb{1}\left\{\max\left\{\left(t - nT_M - \theta\right), \left(s - nT_M - \theta\right)\right\} < 0\right\} \tag{4.35}$$

Then, applying the same computational steps between (4.25) and (4.26) on (4.35) for LEPWM, yields that:

$$\mathbb{E}_\theta \left[\sum_{n=-\infty}^{\infty} S_v(n) \right] = \frac{1}{T_M} \int_{-\infty}^{\infty} \Phi\left(\gamma - \min\left\{\tau, 0\right\}\right) \mathbb{1}\left\{\max\left\{\tau, 0\right\} < \gamma\right\} \, d\gamma$$

Expanding the cases for $\tau > 0$ and $\tau < 0$ yields the identical variance characteristics to those of TEPWM:

$$\mathbb{E}_\theta \left[\sum_{n=-\infty}^{\infty} S_v(n) \right] = \frac{1}{T_M} \int_{|\tau|}^{\infty} \Phi\left(\gamma\right) \, d\gamma \tag{4.36}$$

Therefore, the second moment of a randomized starting point LEPWM has the following form:

$$R_{P_{LE}}(\tau) = \frac{1}{T_M} \left[\sum_{\substack{n=-\infty \\ n \neq 0}}^{\infty} \left(\check{\Phi} * \hat{\Phi} \right)\left(\tau - nT_M\right) + \int_{|\tau|}^{\infty} \Phi\left(\gamma\right) \, d\gamma \right] \tag{4.37}$$

Similar to every analysis that we have conducted hitherto, compared to fixed edge PWM processes, the DEPWM process has different second moment characteristics as well. Although the mechanics behind the computation of the second moment are similar to those for TEPWM and LEPWM, we observe a set of unique behaviors, which we emphasize next. We begin the derivation with the separation of correlation and variation terms:

$$R_{P_{DE}}(t,s) = \mathbb{E}_\theta \left[\mathbb{E}_{W|\theta} \left[\sum_{k=-\infty}^{\infty} \mathbb{1} \left\{ kT_M - \frac{W_k}{2} < t - \theta < kT_M + \frac{W_k}{2} \right\} \sum_{l=-\infty}^{\infty} \mathbb{1} \left\{ lT_M - \frac{W_l}{2} < s - \theta < lT_M + \frac{W_l}{2} \right\} \right] \right]$$

$$= \mathbb{E}_\theta \left[\sum_{\substack{k=-\infty \\ k \neq l}}^{\infty} \sum_{l=-\infty}^{\infty} S_c(k,l) \right] + \mathbb{E}_\theta \left[\sum_{n=-\infty}^{\infty} S_v(n) \right]$$

where for DEPWM, the correlation terms $S_c(k,l)$ and the variation terms $S_v(n)$ are indicator functions on random variables only and are as follows:

$$S_c(k,l) = \mathbb{E}_{W|\theta} \left[\mathbb{1} \left\{ W_k > 2 \left| t - kT_M - \theta \right| \right\} \mathbb{1} \left\{ W_l > 2 \left| s - lT_M - \theta \right| \right\} \right] \tag{4.38}$$

$$S_v(n) = \mathbb{E}_{W|\theta} \left[\mathbb{1} \left\{ W_n > 2 \left| t - nT_M - \theta \right| \right\} \mathbb{1} \left\{ W_n > 2 \left| s - nT_M - \theta \right| \right\} \right] \tag{4.39}$$

Since W_k are i.i.d. for $k \neq l$, (4.38) is separable, which yields that:

$$S_c(k,l) = \Phi\left(2 \left| t - kT_M - \theta \right|\right) \Phi\left(2 \left| s - lT_M - \theta \right|\right)$$

One should observe here that there are no deterministic impositions either in correlation or in variation terms. Therefore, the sum of the correlation terms has a distinct form:

$$\mathbb{E}_\theta \left[\sum_{\substack{k=-\infty \\ k \neq l}}^{\infty} \sum_{l=-\infty}^{\infty} S_c(k,l) \right] = \mathbb{E}_\theta \left[\sum_{\substack{k=-\infty \\ k \neq l}}^{\infty} \sum_{l=-\infty}^{\infty} \Phi\left(2 \left| t - kT_M - \theta \right|\right) \Phi\left(2 \left| s - lT_M - \theta \right|\right) \right]$$

Imposing the expectation first yields that:

$$= \sum_{\substack{k=-\infty \\ k \neq l}}^{\infty} \sum_{l=-\infty}^{\infty} \mathbb{E}_\theta \left[\Phi\left(2 \left| t - kT_M - \theta \right|\right) \Phi\left(2 \left| s - lT_M - \theta \right|\right) \right]$$

Since $\Theta \sim \text{Unif}[0, T_M]$, the expectation definition yields that:

$$= \sum_{\substack{k=-\infty \\ k \neq l}}^{\infty} \sum_{l=-\infty}^{\infty} \int_0^{T_M} \frac{1}{T_M} \Phi\left(2 \left| t - kT_M - \theta \right|\right) \Phi\left(2 \left| s - lT_M - \theta \right|\right) d\theta$$

48

For a fixed l and remaining loyal to the definitions of $\tau = t - s$ and $n = k - l$, we allow $\alpha = 2(s - lT_M - \theta)$, yielding that:

$$\mathbb{E}_\theta \left[\sum_{\substack{k=-\infty \\ k \neq l}}^{\infty} \sum_{l=-\infty}^{\infty} S_c(k,l) \right] = \sum_{l=-\infty}^{\infty} \sum_{\substack{n=-\infty \\ n \neq 0}}^{\infty} \int_{2(s-(l+1)T_M)}^{2(s-lT_M)} \frac{1}{2T_M} \Phi \left(2 \left| \tau - nT_M - \frac{\alpha}{2} \right| \right) \Phi \left(|\alpha| \right) \, d\alpha$$

Changing the order of summation and imposing the definition of $\tilde{\Phi}(t) = \Phi(|t|)$ yield that:

$$= \frac{1}{2T_M} \sum_{\substack{n=-\infty \\ n \neq 0}}^{\infty} \int_{-\infty}^{\infty} \tilde{\Phi}(2(\tau - nT_M) - \alpha) \tilde{\Phi}(\alpha) \, d\alpha$$

Since the integral in the summation argument is a convolution integral, we can formulate the sum of correlation terms as follows:

$$\mathbb{E}_\theta \left[\sum_{\substack{k=-\infty \\ k \neq l}}^{\infty} \sum_{l=-\infty}^{\infty} S_c(k,l) \right] = \frac{1}{2T_M} \sum_{\substack{n=-\infty \\ n \neq 0}}^{\infty} \left(\tilde{\Phi} * \tilde{\Phi} \right) (2(\tau - nT_M)) \tag{4.40}$$

With the correlation terms formulated, we turn our attention to the variation terms. We again start with separable impositions.

$$S_v(n) = \mathbb{E}_{W|\theta} \left[\mathbb{1} \left\{ W_n > 2 \left| t - nT_M - \theta \right| \right\} \mathbb{1} \left\{ W_n > 2 \left| s - nT_M - \theta \right| \right\} \right]$$

$\forall n \in \mathbb{Z}$, there are two conditions on a single random variable. Therefore,

$$= \mathbb{E}_{W|\theta} \left[\mathbb{1} \left\{ W_n > 2 \max \left\{ \left| t - nT_M - \theta \right|, \left| s - nT_M - \theta \right| \right\} \right\} \right]$$

$$= \mathbb{P}_{W|\theta} \left\{ W_n > 2 \max \left\{ \left| t - nT_M - \theta \right|, \left| s - nT_M - \theta \right| \right\} \right\}$$

Applying the definition for the complementary CDF:

$$S_v(n) = \Phi \left(2 \max \left\{ \left| t - nT_M - \theta \right|, \left| s - nT_M - \theta \right| \right\} \right)$$

Therefore, the sum of all variation terms has the following form:

$$\mathbb{E}_\theta \left[\sum_{n=-\infty}^{\infty} S_v(n) \right] = \mathbb{E}_\theta \left[\sum_{n=-\infty}^{\infty} \Phi \left(2 \max \left\{ \left| t - nT_M - \theta \right|, \left| s - nT_M - \theta \right| \right\} \right) \right] \tag{4.41}$$

Applying the change of variables $\theta = s - nT_M - \frac{\gamma}{2}$ for a fixed n and then applying the summation on all n yields that:

$$\mathbb{E}_\theta \left[\sum_{n=-\infty}^{\infty} S_v(n) \right] = \frac{1}{2T_M} \int_{-\infty}^{\infty} \Phi \left(\max \left\{ \left| 2\tau - \gamma \right|, \left| \gamma \right| \right\} \right) \, d\gamma$$
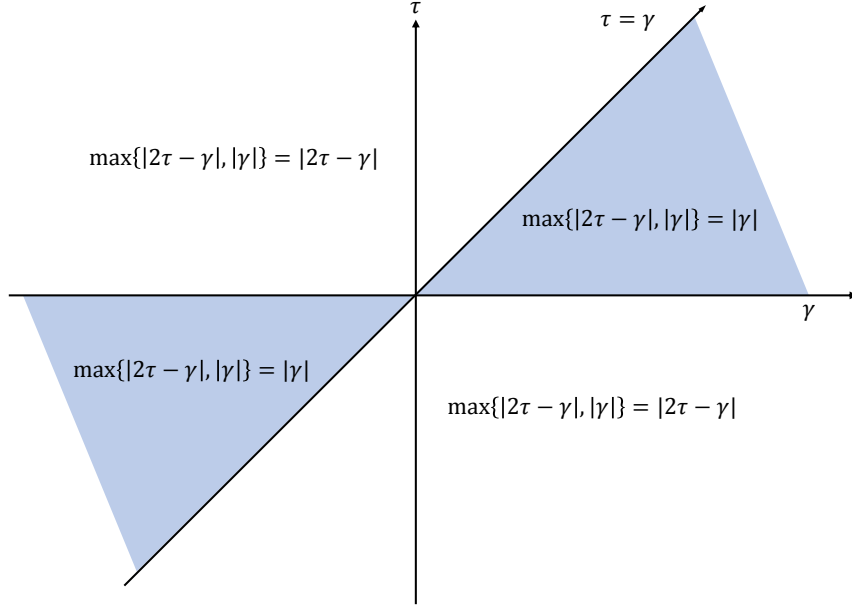
49

Figure 4.1: Outcome Regions of $\max\left\{|2\tau-\gamma|,|\gamma|\right\}$ over γ,τ

At this point, a meticulous effort for simplification is necessary. The analysis starts with the evaluation of $\max\left\{|2\tau-\gamma|,|\gamma|\right\}$ over $\tau,\gamma\in\mathbb{R}$. As Fig. 4.1 indicates:

$$\max\left\{|2\tau-\gamma|,|\gamma|\right\}=\begin{cases}|\gamma| & \text{if } 0<\tau<\gamma \text{ or } \gamma<\tau<0 \\ |2\tau-\gamma| & \text{otherwise}\end{cases} \tag{4.42}$$

Utilizing (4.42), we can formulate the integral separately for $\tau>0$ and $\tau<0$:

$$\int_{-\infty}^{\infty}\Phi\left(\max\left\{|2\tau-\gamma|,|\gamma|\right\}\right)\,d\gamma=\begin{cases}\int_{-\infty}^{\tau}\Phi\left(|2\tau-\gamma|\right)\,d\gamma+\int_{\tau}^{\infty}\Phi\left(|\gamma|\right)\,d\gamma & \text{if } \tau>0 \\ \int_{-\infty}^{\tau}\Phi\left(|\gamma|\right)\,d\gamma+\int_{\tau}^{\infty}\Phi\left(|2\tau-\gamma|\right)\,d\gamma & \text{if } \tau<0\end{cases}$$

Applying the change of variables $\alpha=2\tau-\gamma$ yields:

$$=\begin{cases}2\int_{\tau}^{\infty}\Phi\left(|\alpha|\right)\,d\alpha & \text{if } \tau>0 \\ 2\int_{-\infty}^{\tau}\Phi\left(|\alpha|\right)\,d\alpha & \text{if } \tau<0\end{cases}$$

Since both of the integrations depend on the absolute value of the limits, the main integral reduces to a simple form $\forall\tau\in\mathbb{R}$:

$$\int_{-\infty}^{\infty}\Phi\left(\max\left\{|2\tau-\gamma|,|\gamma|\right\}\right)\,d\gamma=2\int_{|\tau|}^{\infty}\Phi\left(\alpha\right)\,d\alpha$$

50

With this simplification, the second moment of a randomized starting point DEPWM process is as follows:

$$R_{P_{DE}}(\tau) = \frac{1}{T_M} \left[\frac{1}{2} \sum_{\substack{n=-\infty \\ n \neq 0}}^{\infty} \left(\tilde{\Phi} * \tilde{\Phi} \right) (2(\tau - nT_M)) + \int_{|\tau|}^{\infty} \Phi(\alpha) \, d\alpha \right] \tag{4.43}$$

As (4.30), (4.37) and (4.43) indicate, the second moments of a PWM process with a randomized starting point, as defined in (4.11)-(4.13) are functions of time difference τ only. Furthermore, their first moments, as derived in (4.8)-(4.10), are constant in time. Therefore, a PWM process with a randomized starting point is necessarily WSS. In Section 4.3, we demonstrate the accuracy of our results with simulations.

4.3 Simulation Results

In this section, we demonstrate that the second moments formulations are accurate for the case where the pulse widths are independent and uniformly distributed, that is, $W_k \sim \text{Unif}[0, T_M]$, where $T_M = 200$ seconds. First, we postulate the autocorrelation functions using (4.30), (4.37) and (4.43). For uniform distribution, we have the following complementary CDF and its modified versions:

$$\Phi(t) = \begin{cases} 1 & \text{if } t < 0 \\ 1 - \frac{t}{T_M} & \text{if } t \in [0, T_M] \\ 0 & \text{if } t > T_M \end{cases} \qquad \hat{\Phi}(t) = \begin{cases} 1 - \frac{t}{T_M} & \text{if } t \in [0, T_M] \\ 0 & \text{otherwise} \end{cases}$$

$$\check{\Phi}(t) = \begin{cases} 1 + \frac{t}{T_M} & \text{if } t \in [-T_M, 0] \\ 0 & \text{otherwise} \end{cases} \qquad \tilde{\Phi}(t) = \begin{cases} 1 - \left| \frac{t}{T_M} \right| & \text{if } |t| \in [0, T_M] \\ 0 & \text{otherwise} \end{cases}$$

Since $\hat{\Phi}(\cdot)$, $\check{\Phi}(\cdot)$ and $\tilde{\Phi}(\cdot)$ are given above, we can compute the autocorrelation functions given in (4.30), (4.37) and (4.43). First, we need the convolutions $\left(\hat{\Phi} * \check{\Phi} \right)(\cdot)$ and $\left(\tilde{\Phi} * \tilde{\Phi} \right)(\cdot)$, which are given below:

$$\left(\hat{\Phi} * \check{\Phi} \right)(\tau) = \begin{cases} \frac{1}{6} \left(|\tau|^3 - 3|\tau| + 2 \right) & \text{if } |\tau| \in [0, 1] \\ 0 & \text{otherwise} \end{cases} \tag{4.44}$$

$$\left(\tilde{\Phi} * \tilde{\Phi} \right)(\tau) = \begin{cases} \frac{1}{6} \left(3|\tau|^3 - 6|\tau|^2 + 4 \right) & \text{if } |\tau| \in [0, 1] \\ \frac{1}{6} \left(2 - |\tau| \right)^3 & \text{if } |\tau| \in [1, 2] \\ 0 & \text{otherwise} \end{cases} \tag{4.45}$$
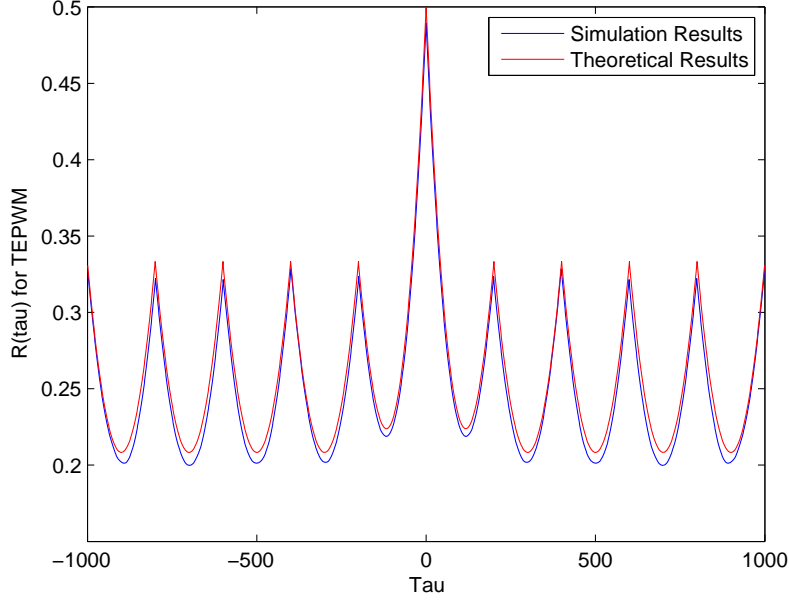
51

Figure 4.2: Comparison between Simulation and $R_{P_{TE}}(\tau)$

With the results in (4.44) and (4.45), we have the exact representation for the autocorrelation functions for the TEPWM and LEPWM cases. As (4.30) and (4.37) indicate, $R_{P_{TE}}(\tau) = R_{P_{LE}}(\tau)$ and they are given as follows:

$$R_{P_{TE}}(\tau) = R_{P_{LE}}(\tau) = \sum_{n=-\infty}^{\infty} q_n\,(\tau - nT)\,\mathbb{1}\,\{nT \leq \tau \leq (n+1)T\} \tag{4.46}$$

where, $q_n(\tau)$ is defined as:

$$
\begin{aligned}
q_0(\tau) &= \frac{-1}{6}\left(\left(\frac{|\tau|}{T}\right)^3 - 6\left(\frac{|\tau|}{T}\right)^2 + 6\left(\frac{|\tau|}{T}\right) - 3\right) \\
q_{n\neq 0}(\tau) &= \frac{1}{6}\left(3\left(\frac{|\tau|}{T}\right)^2 - 3\left(\frac{|\tau|}{T}\right) + 2\right)
\end{aligned}
\tag{4.47}
$$

In the simulations, we have used an unbiased discrete estimator for autocorrelation functions $R_{P_{TE}}(\tau)$ and $R_{P_{LE}}(\tau)$ with $T = 200$ and we have traced the behavior over 10 cycles. As shown in Fig. 4.2 and Fig. 4.3, the simulation results are consistent to the autocorrelation functions given in (4.46) and (4.47). For DEPWM case, the autocorrelation function has the following compact form:

$$R_{P_{DE}}(\tau) = \sum_{n=-\infty}^{\infty} r_n\,(\tau - nT)\,\mathbb{1}\,\{nT \leq \tau \leq (n+1)T\} \tag{4.48}$$
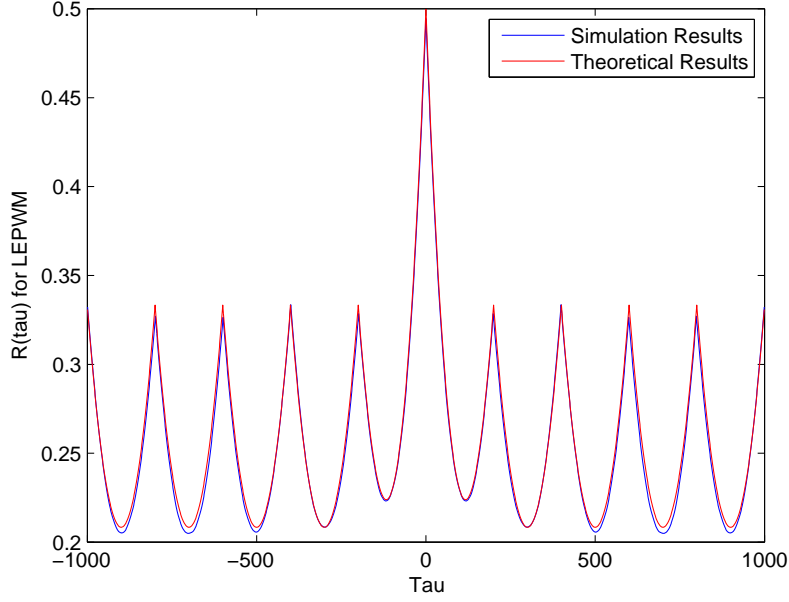
Figure 4.3: Comparison between Simulation and $R_{P_{LE}}(\tau)$

where, for notational simplicity we let $\tilde{\tau} \triangleq \frac{|\tau|-T}{T}$, and then, $r_n(\tau)$ is defined as:

$$r_0(\tau) = \begin{cases} -2\tilde{\tau}^3 - \frac{3}{2}\tilde{\tau}^2 + \frac{1}{3} & \text{if } |\tau| \le \dfrac{T}{2} \\ \frac{2}{3}\tilde{\tau}^3 + \frac{5}{2}\tilde{\tau}^2 - 2\tilde{\tau} + \frac{2}{3} & \text{if } \dfrac{T}{2} \le |\tau| \le T \end{cases} \tag{4.49}$$

$$r_{n\neq 0}(\tau) = \begin{cases} \frac{8}{3}(\tilde{\tau}+1)^3 - 2(\tilde{\tau}+1)^2 + \frac{1}{3} & \text{if } |\tau| \le \dfrac{T}{2} \\ -\frac{8}{3}\tilde{\tau}^3 - 2\tilde{\tau}^2 + \frac{1}{3} & \text{if } \dfrac{T}{2} \le |\tau| \le T \end{cases} \tag{4.50}$$

With the same estimator that we used for the TEPWM and LEPWM cases, we have set $T = 200$ and traced the behavior over 10 cycles. As shown in Fig. 4.4, the simulation results are consistent with the autocorrelation function as given in (4.48)-(4.50).
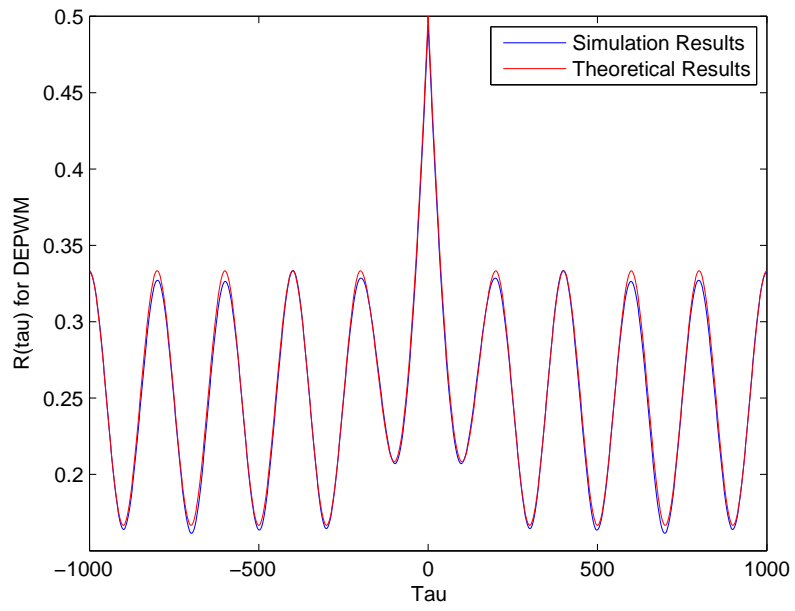
Figure 4.4: Comparison between Simulation and $R_{P_{DE}}(\tau)$

Chapter 5

Conclusion

In this thesis, we have analyzed fundamental properties of a pulse width modulated signal, a classical example among time-domain signals. In this endeavor, we have first analyzed the generation of PWM signals, focusing on the linear and non-linear mappings separately and searching for a foundation to analyze the structural components, which cause a PWM signal to be of infinite energy even when it is generated from a finite energy input signal. In order to analyze the frequency domain representation of the most general PWM case, we have first derived lossless sampling conditions and analyzed the convergence characteristics between natural and uniform sampling. With that intuition, we have chosen low-pass filtering as a linear, suboptimal reconstruction mechanism and proposed an equivalent model to isolate the structural component of the PWM signal at the reconstruction end. Using the frequency domain representation of the signal dependent components of a PWM signal, we have analyzed the performance of low-pass filtering as a function of the oversampling factor, which allowed us to reveal a trade-off between generator complexity and distortion attenuation. After the frequency domain analysis we have turned our attention to stochastic modeling of PWM processes, where we have introduced a randomized starting point to preserve wide-sense stationarity of the input signal and analyzed the stochastic characteristics of the WSS model. The notable details in this sequence of analysis are presented next.

The mathematical modeling of PWM generation entails linear mappings, which consist of the mapping between input samples and pulse widths in addition to the mapping from pulse widths to rising and falling edge instances, and a non-linear mapping where the PWM signal is generated from the rising and falling edge instances. Provided that lossless sampling conditions are satisfied, a comparator with a periodic reference signal can generate a PWM signal, from which perfect reconstruction of the band-limited finite energy input signal is possible. We have shown that if the period of the reference signal satisfies the Nyquist criterion and it spans the input signal range with a factor $C \geq \frac{\pi}{2}$, then natural sampling is lossless. These conditions have allowed us to compare uniform sampling and natural sampling as two lossless sampling operations and motivated us to investigate their convergence characteristics. We postulated a continuous, finite energy, band-limited input signal model from a finite-dimensional signal space to ensure convergence to zero in

tail regions. For lossless sampling, we derived bounds for absolute deviation between natural and uniform samples and the corresponding sampling instances. The bounds on convergence characteristics indicated that the uniform and natural samples converge to each other in $\mathcal{O}\left(\frac{1}{n}\right)$ where the energy in the absolute deviation signal diminishes in the oversampling factor M, within a constant. We further observed that the affine mapping that the sawtooth reference signal imposes manifested itself as a constant difference between natural and uniform sampling instances, which motivated the separation approach that we have proposed.

Then, we have observed that the comparator construction introduces a DC offset to the input signal which manifests itself as a square wave in the modulated signal. Isolating the square wave has allowed us to analyze frequency domain representations of different PWM constructions. Analyzing the deviation from the square wave, which is the information-bearing part of the PWM signal, we have uncovered that low-pass reconstruction introduces a pass-band distortion which diminishes quadratically in the oversampling factor. We have further shown that fixed-edge PWM constructions introduce a time shift of half the symbol interval to the output signal where DEPWM construction makes the input signal blurry by shifting the output signal to right and left by a delay of a quarter of the symbol interval and then normalizing. Nevertheless, despite the additional distortion due to the blurring effect, distortion due to low-pass filtering in DEPWM construction has proven to be diminishing substantially faster in the oversampling factor. In fact, distortion energy due to the low-pass reconstruction of a DEPWM signal diminishes in the oversampling factor as $\mathcal{O}\left(M^4\right)$, where the distortion energy of other constructions diminish in the oversampling factor as $\mathcal{O}\left(M^2\right)$. Therefore, we have observed that there is a trade-off between generator complexity and distortion attenuation for different PWM constructions under low-pass demodulation.

Finally, for different pulse orientations, we have analyzed the stochastic characteristics of a PWM process with independent identically distributed pulse widths. We have first analyzed the characteristics of a PWM process with a fixed starting point and we have shown using first moment calculations that it is not WSS. Then, we have proposed a randomized starting point model for a PWM process, where we have imposed a random variable, independent of the pulse widths and uniformly distributed on a symbol interval as the starting point of the PWM process and shown that a PWM process with a randomized starting point and i.i.d. pulse widths are necessarily WSS. We have further shown that the autocorrelation function of a PWM signal can be represented as a superposition of linear operations over the complementary cumulative distribution functions of pulse widths, which are defined by the input signal under an invertible mapping.

References

[1] H. Black, *Modulation Theory*, ser. Bell Telephone Laboratories series. Princeton, NJ: Van Nostrand, 1953.

[2] R. J. Watts, "Pulse width modulation," U.S. Patent 2,556,457, June 12, 1951.

[3] G. Buja and G. Indri, "Improvement of pulse width modulation techniques," *Electrical Engineering (Archiv fur Elektrotechnik)*, vol. 57, no. 5, pp. 281–289, 1975.

[4] Z. Song and D. V. Sarwate, "The frequency spectrum of pulse width modulated signals," *Signal Processing*, vol. 83, no. 10, pp. 2227–2258, 2003. [Online]. Available: http://www.sciencedirect.com/science/article/pii/S0165168403001646

[5] A. V. Oppenheim and R. W. Schafer, *Discrete-Time Signal Processing*. Prentice-Hall Englewood Cliffs, 1989, vol. 2.

[6] Y.-C. Jenq, "Perfect reconstruction of digital spectrum from nonuniformly sampled signals," *Instrumentation and Measurement, IEEE Transactions on*, vol. 46, no. 3, pp. 649–652, 1997.

[7] R. G. Wiley, "Recovery of bandlimited signals from unequally spaced samples," *Communications, IEEE Transactions on*, vol. 26, no. 1, pp. 135–137, 1978.

[8] P. Marziliano and M. Vetterli, "Reconstruction of irregularly sampled discrete-time bandlimited signals with unknown sampling locations," *Signal Processing, IEEE Transactions on*, vol. 48, no. 12, pp. 3462–3471, 2000.

[9] H. Alasti, "Non-uniform-level crossing sampling for efficient sensing of temporally sparse signals," *IET Wireless Sensor Systems*, vol. 4, no. 1, pp. 27–34, 2013.

[10] U. Grunde and M. Greitans, "Advanced level-crossing sampling method," in *Telecommunications Forum (TELFOR), 2011 19th*. IEEE, 2011, pp. 797–800.

[11] K. M. Guan and A. C. Singer, "Opportunistic sampling of bursty signals by level-crossing-An information theoretical approach," in *Information Sciences and Systems, 2007. CISS'07. 41st Annual Conference on*. IEEE, 2007, pp. 701–707.

[12] C. Henze, H. Martin, and D. Parsley, "Zero-voltage switching in high frequency power converters using pulse width modulation," in *Applied Power Electronics Conference and Exposition, 1988. APEC'88. Conference Proceedings 1988, Third Annual IEEE*. IEEE, 1988, pp. 33–40.

[13] D. G. Holmes and T. A. Lipo, *Pulse Width Modulation for Power Converters: Principles and Practice*. John Wiley & Sons, 2003, vol. 18.

[14] A. M. Trzynadlowski, S. Legowski, and R. Lynn Kirlin, "Random pulse-width modulation technique for voltage-controlled power inverters," *International Journal of Electronics*, vol. 68, no. 6, pp. 1027–1037, 1990. [Online]. Available: http://dx.doi.org/10.1080/00207219008921243

[15] A. M. StankoviÄ, "Random pulse modulation with applications to power electronic converters," Ph.D. dissertation, Massachusetts Institute of Technology, 1993.

[16] J. Holtz, "Pulsewidth modulation for electronic power conversion," *Proceedings of the IEEE*, vol. 82, no. 8, pp. 1194–1214, 1994.

[17] T. Bruckner and D. G. Holmes, "Optimal pulse-width modulation for three-level inverters," *Power Electronics, IEEE Transactions on*, vol. 20, no. 1, pp. 82–89, 2005.

[18] R. Kirlin, S. Kwok, S. Legowski, and A. Trzynadlowski, "Power spectra of a PWM inverter with randomized pulse position," *Power Electronics, IEEE Transactions on*, vol. 9, no. 5, pp. 463–472, Sep 1994.

[19] P. C. Loh, D. M. Vilathgamuwa, Y. S. Lai, G. T. Chua, and Y. Li, "Pulse-width modulation of z-source inverters," in *Industry Applications Conference, 2004. 39th IAS Annual Meeting. Conference Record of the 2004 IEEE*, vol. 1. IEEE, 2004.

[20] C. Pascual, Z. Song, P. Krein, D. Sarwate, P. Midya, and W. Roeckner, "High-fidelity PWM inverter for digital audio amplification: Spectral analysis, real-time DSP implementation, and results," *Power Electronics, IEEE Transactions on*, vol. 18, no. 1, pp. 473–485, Jan 2003.

[21] M. Mansuripur, *The Physical Principles of Magneto-Optical Recording.* Cambridge: Cambridge University Press, 1998.

[22] S. Suh, "Pulse width modulation for analog fiber-optic communications," *Lightwave Technology, Journal of*, vol. 5, no. 1, pp. 102–112, 1987.

[23] S. Rao, B. Young, A. Elshazly, W. Yin, N. Sasidhar, and P. K. Hanumolu, "A 71db SFDR open loop VCO-based ADC using 2-level PWM modulation," in *VLSI Circuits (VLSIC), 2011 Symposium on.* IEEE, 2011, pp. 270–271.

[24] S. Z. Asl, S. Saxena, P. K. Hanumolu, K. Mayaram, and T. S. Fiez, "A 77db SNDR, 4mhz MASH $\Delta\Sigma$ modulator with a second-stage multi-rate VCO-based quantizer," in *Custom Integrated Circuits Conference (CICC), 2011 IEEE.* IEEE, 2011, pp. 1–4.

[25] K. Reddy, S. Rao, R. Inti, B. Young, A. Elshazly, M. Talegaonkar, and P. K. Hanumolu, "A 16-mw 78-db SNDR 10-MHz BW CT ADC using residue-cancelling VCO-based quantizer," *Solid-State Circuits, IEEE Journal of*, vol. 47, no. 12, pp. 2916–2927, 2012.

[26] J. Holtz, "Pulsewidth modulation-A survey," *Industrial Electronics, IEEE Transactions on*, vol. 39, no. 5, pp. 410–420, 1992.

[27] A. Papoulis, *Signal Analysis.* McGraw-Hill New York, 1978, vol. 191.

[28] M. Vetterli, J. Kovačević, and V. Goyal, *Foundations of Signal Processing.* Cambridge: Cambridge University Press, 2014. [Online]. Available: http://books.google.com/books?id=MJzCnAEACAAJ

[29] J. M. Steele, *The Cauchy-Schwarz Master Class: An Introduction to the Art of Mathematical Inequalities.* New York, NY, USA: Cambridge University Press, 2004.

[30] B. Hajek, *An Exploration of Random Processes for Engineers.* Urbana, IL: Department of Electrical and Computer Engineering at the University of Illinois at Urbana-Champaign, 2009.